

1 **VARIATIONS IN TROPOSPHERIC SUBMICRON PARTICLE SIZE**
2 **DISTRIBUTIONS ACROSS THE EUROPEAN CONTINENT**
3 **2008-2009**
4

5 **D. C. S. Beddows¹, M. Dall'Osto², Roy M. Harrison^{1*†}, M. Kulmala³,**
6 **A. Asmi³, A. Wiedensohler⁴, P. Laj⁵, A.M. Fjaeraa⁶, K. Sellegri⁷,**
7 **W. Birmili⁴, N. Bukowiecki⁸, E. Weingartner⁸, U. Baltensperger⁸,**
8 **V. Zdimal⁹, N. Zikova⁹, J.-P. Putaud¹⁰, A. Marinoni¹¹, P. Tunved¹²,**
9 **H.-C. Hansson¹², M. Fiebig⁶, N. Kivekäs^{13,14}, E. Swietlicki¹³,**
10 **H. Lihavainen¹⁴, E. Asmi¹⁴, V. Ulevicius¹⁵, P. P. Aalto³, N. Mihalopoulos¹⁶,**
11 **N. Kalivitis¹⁶, I. Kalapov¹⁷, G. Kiss¹⁸, G. de Leeuw^{3, 14,19}, B. Henzing¹⁹,**
12 **C. O'Dowd²⁰, S. G. Jennings²⁰, H. Flentje²¹, F. Meinhardt²², L. Ries²³,**
13 **H.A.C. Denier van der Gon¹⁹, A.J.H. Visschedijk¹⁹**

14
15 ¹ National Centre for Atmospheric Science, School of Geography, Earth and Environmental Sciences, University of
16 Birmingham, B15 2TT, UK

17 ² Institut de Ciències del Mar, CSIC, Pg Marítim de la Barceloneta 37-49 08003 Barcelona, Spain

18 ³ Department of Physics, University of Helsinki, P.O. Box 64, Helsinki, Finland

19 ⁴ Leibniz Institute for Tropospheric Research, Permoserstraße 15, 04318 Leipzig, Germany

20 ⁵ Laboratoire de Glaciologie et Géophysique de l'Environnement Université Joseph Fourier, Grenoble 1/CNRS, 38400 St.
21 Martin d'Hères, France

22 ⁶ NILU - Norwegian Institute for Air Research Instituttveien 18, 2027 Kjeller, Norway

23 ⁷ Laboratoire de Météorologie Physique, UMR 6016, CNRS/University of Clermont-Ferrand, Clermont-Ferrand, France

24 ⁸ Laboratory of Atmospheric Chemistry, Paul Scherrer Institute, 5232 Villigen PSI, Switzerland

25 ⁹ Laboratory of Aerosol Chemistry and Physics, Institute of Chemical Process Fundamentals of the AS CR, v.v.i.,
26 Rozvojova 135, 16502 Praha 6, Czech Republic

27 ¹⁰ European Commission, Joint Research Centre, Institute for Environment and Sustainability, 21027 (VA), Italy

28 ¹¹ CNR-ISAC, Institute of Atmospheric Sciences and Climate, 40129, Bologna, Italy

29 ¹² Department of Applied Environmental Science (ITM), Stockholm University, 10691 Stockholm, Sweden

30 ¹³ Department of Physics, Lund University, SE-22100, Lund, Sweden

31 ¹⁴ Finnish Meteorological Institute, Erik Palménin aukio 1, P.O. Box 503, FI-00101, Helsinki, Finland

32 ¹⁵ Center for Physical Sciences and Technology, Savanoriu 231, 02300 Vilnius, Lithuania

33 ¹⁶ Environmental Chemical Processes Laboratory, Department of Chemistry, University of Crete, Greece

34 ¹⁷ Institute of Nuclear Research and Nuclear Energy, Bulgarian Academy of Sciences, Blvd. Tzarigradsko chaussee, 72,
35 1784 Sofia, Bulgaria

36 ¹⁸ MTA-PE Air Chemistry Research Group, P.O. Box 158, 8201 Veszprém, Hungary

37 ¹⁹ Netherlands Organisation for Applied Scientific Research TNO, Princetonlaan 6, 3508 TA Utrecht, The Netherlands

38 ²⁰ National University of Ireland Galway, University Road, Galway, Ireland

39 ²¹ German Meteorological Service, Hohenpeissenberg Observatory, Albin-Schwaiger Weg 10, 82383 Hohenpeissenberg,
40 Germany

41 ²² German Federal Environment Agency (UBA), Messnetzcentrale, Paul-Ehrlich-str. 29, 63225, Langen, Germany

42 ²³ German Federal Environment Agency (UBA), Plattform Zugspitze of GAW Global Station Zugspitze/
43 Hohenpeissenberg, Zugspitze 5, 28475 Zugspitze, Germany

44
45

* To whom correspondence should be addressed.

Tele: +44 121 414 3494; Fax: +44 121 414 3708; Email: r.m.harrison@bham.ac.uk

† Also at: Department of Environmental Sciences / Center of Excellence in Environmental Studies, King Abdulaziz University, PO Box 80203, Jeddah, 21589, Saudi Arabia

1 **1. INTRODUCTION**

2 Airborne particle size distributions vary in space and time and can be interpreted in terms
3 of known sources, meteorological processes and aerosol dynamical processes affecting
4 such particles. Sources contributing to particle concentrations in the atmosphere are both
5 primary and secondary. Traffic is often found to be the most important primary source for
6 ultrafine particles in urban areas (Charron and Harrison, 2003; Harrison and Jones, 2005).
7 Particles in rural areas are from a wider range of sources, both primary and secondary.
8 New secondary particles formed by nucleation are generated from gas-to-particle
9 conversion. Such particles have been observed at many surface locations around the
10 world and also within the free and upper troposphere (Kulmala et al., 2004; Venzac et al.
11 2008; Boulon et al. 2010, 2011). Reddington et al. (2011) recently stressed the importance
12 of understanding the relative contribution of primary and secondary particles in regional
13 and global aerosol so that models can attribute aerosol radiative forcing to different
14 sources.

15

16 Compliance monitoring of particle mass metrics is widely performed (EEA, 2009), but at
17 present, measurement of particle number concentrations is not required. Nevertheless, as
18 the importance of particle number concentration as a complement to the existing PM_{2.5}
19 and PM₁₀ metrics has become recognised, particle size distributions are increasingly being
20 measured in the context of air quality at multiple locations. For example - at national level -
21 the UK Particle Monitoring Programme operates three SMPS instruments at Harwell (the
22 UK EUSAAR site), and at the London sites of North Kensington and Marylebone Road, all
23 measuring sub-micrometre particle number-size distributions, upon which numerous
24 studies have been based (Charron et al., 2007; Beddows et al., 2009; Harrison et al.,
25 2011). In Germany a similar initiative, established in 2008 by the German Environment

1 Agency and known as the German Ultrafine Aerosol Network (GUAN), brings together
2 several German institutes with an interest in sub-micrometre aerosol properties (Birmili et
3 al., 2009). At European level, the EUSAAR (European Supersites for Atmospheric Aerosol
4 Research) project of the Sixth Framework Programme of the European Commission
5 contributed to development of a harmonised and quality-controlled network of
6 measurements (Philippin et al., 2009; Asmi et al., 2011). The EUSAAR project coordinated
7 24 European sites measuring aerosol chemical, physical and optical properties following a
8 standardised protocol of instrument maintenance, measurement procedures and data
9 delivery using a common format to a single database (Wiedensohler et al., 2012).
10 Recently, the EUSAAR project activities continued within the ACTRIS project (Philippin et
11 al., 2009).

12

13 Asmi et al. (2011) presented a detailed overview of the sites and seasonally disaggregated
14 size distributions collected at the EUSAAR and GUAN stations for the dry diameters
15 between 30 and 500 nm for the years 2008 and 2009. The sites used to collect data are
16 given in Table 1 and the reader is referred to Asmi et al. (2011) for a full account and
17 description. It is important to note that all these sites are considered as remote or rural
18 regional monitoring sites. Data was collected using either Differential Mobility Particle Sizer
19 (DMPS) or Scanning Mobility Particle Sizer (SMPS) instruments and then harmonised into
20 a single dataset.

21

22 Briefly, Asmi et al. (2011) showed that the aerosol concentrations in Europe are highly
23 variable spatially and divide their description into 9 areas: *Central European; Mountain;*
24 *Arctic; Balkans; Nordic, Baltic, North Italian; Mediterranean; Western European* (Figure 1).
25 *Central European aerosol* is observed at the low altitude stations CBW, BOS, WAL, MPZ,

1 OBK and KPO from the Netherlands along a belt of land passing across Germany, Czech
2 Republic, Slovakia to Hungary. These sites measure high concentrations of particles with
3 almost unimodal median distributions but have small seasonal changes. South of this belt
4 are the mountain stations of SSL, HPB, ZSF, JFJ and CMN. The mountain stations of SSL
5 and HPB had many similarities with the low altitude boundary layer measurements and the
6 higher mountains, at lower latitudes (including BEO) whose distributions characterised the
7 *Mountain aerosol*. These had episodes of extremely clean air, most probably from the free
8 troposphere, alternating with episodes of relatively polluted air masses, especially during
9 daytime in summer. The stations with this kind of aerosol were JFJ, BEO, ZSF and CMN.
10 In contrast, the *North Italian aerosol* from site IPR had very high number concentrations,
11 especially during winter in the accumulation mode. Also at the lowest latitude site (FKL), a
12 *Mediterranean aerosol* was measured with maximum number concentrations during
13 summer and spring. At latitudes higher than the Central European belt, the *Northern*
14 *European Aerosol*, had lower concentrations and the seasonal cycle has a strong effect on
15 the particles in this region, and the overall variation is relatively large. The summer
16 concentrations were usually greatest, especially for smaller particle sizes. The
17 concentration distributions often show multiple modes, suggesting a combination of more
18 polluted air masses, and cleaner air from the Arctic or Atlantic oceans. The stations
19 included in this group were BIR, VHL, ASP and SMR. PAL has many similarities with other
20 Nordic stations and had even more extreme seasonal variation and thus had some
21 parameters in common with Arctic aerosol concentrations and variability. The Baltic PLA
22 station was only partially similar to the Nordic stations, with both concentration histograms
23 and size distributions showing influence from multiple source areas of particles and some
24 similarities in concentration levels with Central European aerosol. The *Arctic aerosol*, with
25 high seasonality, was observed at ZEP with very low number concentrations and evidence

1 of Arctic haze events during dark winter periods. Then finally, the *Western European*
2 aerosol (MHD, PDD and HWL) showed clear influence of multiple sources of aerosol
3 (clean and polluted), and with a strong seasonal cycle for smaller particle sizes.

4
5 The study of Asmi et al. (2011) is a landmark study in unifying particle size distribution data
6 and average particle number concentrations. In this current work, we further extend the
7 analysis by applying *k*-means cluster analysis to the particle size distributions (Beddows et
8 al., 2009). A great advantage of this clustering method over the provision of average of
9 aerosol size distributions (Asmi et al., 2011) is that it can provide a small number of size
10 distributions, which can be compared across different time periods. Accordingly, the final
11 cluster centres reflect particle number size distributions representative of each cluster. In
12 other words, the clustering reduces the complexity of the dataset and this simplification
13 allows easier separation of different size distributions from a single site, intercomparison of
14 these distributions across sites, and interpretation of aerosol dynamical processes as
15 aerosol is advected across Europe.

16

17 **2. METHODOLOGY**

18 Although the instruments within the 24 site network of SMPS/DMPS devices used several
19 different size ranges, all the data collected were harmonised into one large matrix by
20 interpolating the data onto a common size bin scale; 121 size bins spanning 1 to 1000 nm
21 with 40 channels per decade were used. Not all instruments shared the same size range
22 or used the same size bins, hence blank lower and upper columns were trimmed from
23 this matrix until every element had a value. In all, the reduced matrix had 54 size bins

1 (17.8 – 375.8 nm) and 117,000 hourly particle size spectra (given the capture rates of the
2 instruments across the EUSAAR network in 2008/9).

3
4 The data are extracted from the EBAS database (<http://ebas.nilu.no>), located at NILU -
5 Norwegian Institute for Air Research, which is a database hosting data for projects and
6 programmes such as the European Monitoring and Evaluation Programme (EMEP), the
7 Global Atmospheric Watch - World Data Centre for Aerosols (GAW-WDCA) and the
8 European Aerosol, Clouds and Trace gases Research InfraStructure network
9 (ACTRIS). The EBAS data was collected under UTC (Temps Universel Coordonné) and had
10 a time resolution of 1 hour and it was initially deemed preferable to cluster at this
11 resolution. However, the method proposed by Beddows et al. (2009) to determine the
12 optimum number of k -Means clusters in Cran R (R Development Core Team, 2011), has a
13 limited capacity to hold particle size spectra (~5000 spectra per analysis running on a 32bit
14 PC). Consequently, the data were analysed at hourly resolution using a giant data set
15 clustering strategy (see section 2.1) and then further reduced in number by averaging the
16 spectra over different time periods (daily, weekly).

17
18 In order to group the data into a manageable number of groups, the data set (consisting of
19 either hourly, daily or weekly averaged spectra) was analysed using k -means cluster
20 analysis (Beddows et al., 2009). Given that S_k represents the set of spectra in the k^{th}
21 cluster and $\overline{spectrum_{k,m}}$ represents the mean for the particle size bin mobility diameter m
22 over cluster k , the k -means method partitions the data into G groups such that the ‘within-
23 cluster sum of squares’ expression is minimised using an iterative cycle, Eq (1).

24

$$\sum_{k=1}^G \sum_{d \in S_k} \left\| \text{spectrum}_{d,m} - \overline{\text{spectrum}_{k,m}} \right\|^2$$

1

1

2 Known as the Hartigan and Wong (1979) method, this starts with a random initial partition
3 and continually reassigns the particle size spectra to the clusters based on the similarity
4 between the spectra and the cluster centers until a convergence criterion is met. The
5 particle size distributions were normalised to their unit length in order to cluster shapes
6 rather than clustering shapes of different magnitudes which would significantly increase
7 the number of clusters.

8

9 **2.1 Hourly Data**

10 For the analysis on an hourly resolution, we successfully tested the k -means functions
11 provided in the CRAN R-Package BIRCH (Balanced Iterative Reducing and Clustering
12 using Hierarchies). This package is used when dealing with very large data sets and it
13 does not require that the data can fit in physical memory. BIRCH is an implementation of
14 the algorithms described in Zhang et al. (1997), and provides functions for creating
15 Clustering Feature Trees, along with algorithms for applying k -means clustering (although
16 limited to 30 size bins). This resulted in a 9 cluster result optimized using an RSS value
17 (i.e. the total residual sum-of-squares of the clustering). However, the diurnal shifts in
18 modal diameter are lost when clustering hourly spectra (see Figures S1 and S2). Even
19 though cluster maxima and minima are evident over an average daily cycle when using
20 hourly spectra, there is a tendency for each cluster result to be constrained to its mean
21 spectrum type and thus dividing diurnal trends in the modal diameter over more than one
22 cluster.

23

1 **2.2 Daily Data**

2 In contrast to hourly data, a better solution was found with the daily averaged data. To
3 determine the optimum number of clusters, a random selection of 5000 daily spectra was
4 used indicating an optimum of 9 clusters which gave a maximum in the Dunn Indices (6.45
5 $\times 10^{-4}$) and a Silhouette Width of 0.363 (Beddows et al, 2009). Subsequently the pre-
6 normalised particle size spectra were partitioned into 9 groups using the cluster analysis
7 assignments (1,2,...,9) yielded from the clustering of the normalised data using a setting of
8 $G = 9$. Furthermore, even though daily average spectra were clustered, the average
9 spectra making up these days could be disaggregated to form average hourly spectra for
10 each cluster so that the diurnal variation of each could be understood and used to help
11 characterize each cluster. This was considered to be one of the main strengths of this new
12 approach.

13

14 **2.3 Weekly Data**

15 This same strategy can then be applied to weekly averaged spectra to reveal
16 weekday/weekend trends as well as seasonal trends (see results in Figures S3 and S4).

17

18 In summary, when clustering daily and weekly averaged spectra, particle growth behaviour
19 is preserved and is visible over the plotted average - which can then be used to provide an
20 improved characterization of the cluster.

21

22 **3. RESULTS**

23 **3.1 Overview of the Particle Size Distribution Clustering**

24 By clustering all of the spectra collected across the 24 EUSAAR sites, an understanding of

1 how the spectrum types are shared between these sites can be observed. The daily
2 spectra collected at each of the 24 EUSAAR sites over the years 2008 and 2009 can be
3 summarised in nine *k*-means clusters (see Figure 2). Six show strong ultrafine modes
4 (Cluster 1, 2, 5, 6, 7 and 8 have modal-diameter < 100 nm) and three show accumulation
5 modes (Cluster 3, 4 and 9 have modal-diameter > 100 nm).

6

7 Considering the size distributions, spatial patterns and temporal behaviour of the individual
8 clusters in relation to the above sources and aging processes, examination of the particle
9 size spectra in Figure 2 suggests the following:

10

- 11 • Clusters 5 and 1 are associated mainly with nucleation processes. Cluster 1 appears
12 more aged, as it contains a greater component of particles at larger diameters than
13 Cluster 5.
- 14 • Clusters 9, 3 and 4 (modal diameters > 0.1 μm) represent well aged accumulation
15 mode particles.
- 16 • Cluster 6 (modal diameter 30-40 nm) is similar to the spectrum of freshly emitted
17 road traffic exhaust, but given the rural or remote locations of the sampling sites,
18 probably has other origins or comprises aged nucleation particles.
- 19 • Clusters 7, 8 and 2 lie in the range between the nucleation/combustion emission
20 spectra and the accumulation mode spectra and probably represent intermediate
21 aging or multiple mixed sources.

22

23 In Figures 3 and S5 the cluster frequencies are plotted for each site. In Figure 3, the sites
24 have been grouped according to geographic factors (location, altitude, etc) and show

1 considerable similarities in pattern between sites within the same group. Features
2 apparent are:

- 3 • Cluster 5, with the smallest modal diameter and more clearly indicative of nucleation
4 appears most frequently at the cleaner sites: MHD, PAL, CMN, PDD, SMR and ZSF,
5 including several of the high altitude sites.
- 6 • Cluster 1 shows a wider abundance, including relatively high frequencies at BOS,
7 HBP, MHD, MPZ, PDD, SSL and ZSF, possibly reflecting nucleation in slightly more
8 polluted air masses.
- 9 • Cluster 6 appears frequently at BIR, CMN, HWL, JFJ, PAL, PDD, SMR and may
10 represent either fresh combustion emissions, or given the remote locations of most of
11 the sites, probably represents aged nucleation particles.
- 12 • Clusters 7, 8 and 2 which have modes between the nucleation group (i.e. > 35 nm)
13 and the accumulation mode group Cluster 9 (< 0.11 μm) appear more frequently at
14 BIR, BOS, CBW, CMN, HBP, HWL, IPR, JFJ, KPO, MPZ, PAL, PDD, SMR, SSL,
15 VHL, WAL, ZSF (i.e. almost all sites), with a clear distinction between those with a
16 high frequency of Cluster 2 and those with mainly Cluster 7 and 8. The reasons for
17 this are unclear.
- 18 • Clusters 9, 3 and 4 representing clear accumulation mode particles appear frequently
19 at BEO, CMN, FKL (Cluster 9 only), HBP (Cluster 3 only), IPR (Cluster 9 only), KPO,
20 MHD (Cluster 3 only), MPZ (Cluster 3 only), OBK, PLA (Cluster 9 only), SMR, SSL
21 (Cluster 3 only), VHL, ZSF and most notably at ZEP where the frequency of Cluster 4
22 far exceeds that of all others.

23

1 The overall conclusion of these results appears to be that nucleation affects all sites, but is
2 common at only a few sites, and all sites experience aged aerosol to differing degrees.
3 This is unsurprising in the context of atmospheric transport and the geography of Europe.

4
5 Figure 4 shows these modes in more detail and how the spectra vary across the quartile
6 plots. For each cluster, the colour plots also show the dependence of the particle size
7 spectra on the hour of the day and in this case, the benefits of clustering the daily average.
8 Also shown are the monitoring sites at which the clusters are most frequently observed
9 (See European maps in Figure 4 and also Figure S5 which shows the frequency of
10 occurrence at each site with latitude and longitude). In general when referring to Figure 4,
11 the broader multimodal distributions (Clusters 1-3) are most frequently detected in central
12 Europe, where there are likely to be many source regions influencing a site, whereas the
13 remaining narrower distributions are most frequently detected at the Northern, Western
14 and Eastern European sites. The nucleation modes tend to be most frequently observed
15 at the higher latitude sites North of, and West of, the industrial heart of Europe.

16
17 Clusters that show a temporal pattern likely to be associated with nucleation are Clusters
18 1, 2, 3, 5 and 6. These are characterised by an increase in particle numbers in the
19 smallest size range (below 20 nm) at around 15:00 hours (UTC) with a mode that
20 increases in size through the following hours (Figure 4). Figure S6 shows that these
21 clusters show very different seasonal patterns. Clusters 1, 3, 5 and 4 have a higher
22 percentage of occurrence during the winter months, whereas Clusters 6, 7 and 8 tend to
23 have a higher occurrence during the summer months. Cluster 2 and 9 do not show a clear
24 seasonal trend. At ZEP, Cluster 4 is most prominent over the winter, detected between
25 September and April whereas Cluster 5 is observed mainly in the summer between March

1 and August. This is in approximate agreement with the seasonal averages reported by
2 Asmi et al. (2011) and Ström et al. (2003) who attributed the accumulation mode
3 distributions to Arctic Haze and the Aitken mode distributions to photochemical processes.
4 At MHD, Cluster 5 peaks in April and September and is at a minimum during the winter
5 months. Cluster 5, which shows a mode at one of the smallest diameters, may be
6 consistent with nucleation processes. At some of the more remote sites (e.g. ZEP),
7 Cluster 5 is observed mainly in the summer between March and August, but overall tends
8 to show higher frequency in the cooler months. Since seasonal frequencies of nucleation
9 vary across Europe, this may be the result of nucleation processes, but points to the fact
10 that a given cluster may have more than one mechanism of genesis. Since Clusters 1, 2,
11 3 and 6, which show the most obvious temporal growth process apparently driven by solar
12 radiation followed by condensational growth at the colder temperatures in the evening,
13 have a wide range of modal diameters, it seems probable that the common feature is that
14 they are undergoing growth rather than necessarily being newly formed. Indeed, all of
15 these distributions show marked breadth and include separate modes obscured by the
16 overall umbrella curve. Clusters 1, 2 and 3 all show a dominance of central European
17 sites and also of mountain sites, presumably reflecting the relatively high concentration of
18 potential substrates for gas-to-particle conversion processes or low condensation sink.
19 Clusters 7 and 4 show predominant association with a single site. In the case of Cluster 7,
20 most frequently measured at CBW, the size distribution is strongly suggestive of an aged
21 vehicle exhaust aerosol in which the semi-volatile particles have evaporated leaving
22 predominantly the larger non-volatile particles (Dall'Osto et al 2011b). The presence of
23 CBW in the heavily urbanised area of the Netherlands is consistent with such an
24 explanation, although a number of Scandinavian sites in very much less polluted areas are
25 also associated with this cluster. In the case of Cluster 4, one site (ZEP) accounts for

1 around 50% of observations (Figure S5) both in summer and winter. Cluster 4 shows a
2 very strong association with the winter months (Figure S6) and a very coarse modal
3 diameter at around 150 nm. This appears to be a strongly aged accumulation mode
4 aerosol associated with the Arctic haze phenomenon. Clusters 4 and 9, both of which
5 represent clusters with relatively coarse modes show their highest abundance during
6 nocturnal hours, presumably associated with low level nocturnal inversions and
7 condensational growth.

8

9 **3.2 Categorization of the Nine Clusters by Cluster Proximity Diagram**

10 The results can also be generalised by the Cluster Proximity Diagram in Figure 5 for UTC.
11 While *k*-means clustering matches together the most similar spectra into the nine clusters,
12 the Cluster Proximity Diagram positions these clusters according to the degree of similarity
13 that each cluster has to each other. In other words, the closer the clusters are in the
14 diagram, the more similar they are (Figure 5). So for instance, Clusters 5 and 4 contain the
15 most different spectra and hence there are at least 2 other clusters in between them on the
16 diagram, whereas Clusters 2 and 8 are more similar. In essence, clusters next to each
17 other on the diagram are similar to each other but not sufficiently similar to form a new
18 cluster if merged. When arranging the clusters in this manner (represented by 9 nodes in
19 the diagram) trends can be extracted from the data. In this diagram, it can be seen that
20 both the modal diameter of the clusters and the hour of the day at which the cluster
21 reaches its maximum particle number concentration increases from left to right. These
22 trends become evident when the modal diameter is plotted as a function of hour of
23 maximum particle number concentration (Figure 6).

24

25 The clusters furthest apart on the Cluster Proximity Diagram, Clusters 5 and 4 have a

1 geographic Arctic/Atlantic signature. However, their separation in the Cluster Proximity
2 Diagram is due to the fact that whilst Cluster 5 is the beginning of category representing
3 the general movement of an air mass from West to East, Cluster 4 is the end product of
4 another category representing the general movement of air mass from South to North. The
5 cluster with the smallest modal diameter (Cluster 5, ~22 nm) occurs with greatest
6 frequency at the coastal site of MHD and at the Arctic and Nordic sites of ZEP, PAL and
7 SMR (see Tunved et al., 2012). In contrast, Cluster 4 is also most commonly observed at
8 ZEP and then PAL and SMR but has much larger modal diameter of 0.16 μm .

9
10 Clusters 1, 2 and 3 are all linked together and occur most frequently in Central Europe.
11 The low altitude MPZ and mid altitude SSL site are common to all of Clusters 1-3 as
12 maximum occurrence sites. Clusters 1 and 2 exhibit similar characteristics in that both
13 are nucleation mode clusters which enter the measurement size range during the
14 afternoon as small particles due to photochemical processing of gases and then develop
15 into larger particles in the evening and night time hours (see Figure 4, colour map) and
16 potentially sharing the same processes since Clusters 1 and 2 share the same sites of
17 occurrence with the exception of MHD and VHL. Furthermore, the presence of Cluster 1
18 at MHD may indicate the influence of nucleation of particles in marine air (in the lower
19 percentiles of the cluster) which then age as they move inland. The average spectrum of
20 Cluster 3 is centred above 0.1 μm and shares a similar 24 hour characteristic in its colour
21 map as Clusters 1 and 2 suggesting that at some sites, this cluster occurs partly as a
22 consequence of the presence of events and processes within Clusters 1 and 2.

23
24 At the furthest right hand of the cluster proximity-diagram are Clusters 4 and 9 which
25 include spectra from the later part of the aging process as the air moves on average from

1 South to North or West to East. Cluster 9 is frequently observed in the two most easterly
2 observatories BEO and FKL supporting the generalisation that as the air masses move to
3 greater longitudes, the modal diameter of the size distribution increases as the air mass
4 passes over the land (see Figure 7 and S7). Considering the site of Finokalia (FKL),
5 Cluster 9 occurs throughout the year, being most prominent at this site during the months
6 March, April and May. The colour map shows it to occur most during the night when the
7 boundary layer is at its shallowest. This distribution typifies the aged and polluted aerosol
8 distributions commonly observed in the eastern Mediterranean (Eleftheriadis et al. 2006;
9 Hildebrandt et al., 2010; Kopanakis et al., 2013). Cluster 9 is also detected frequently
10 during the summer at BEO and KPO. However, at ASP and SMR, the spectra in this
11 cluster are more frequent during the Winter-Spring time (January-July). Although Cluster 4
12 is measured at BEO and FKL, it is most frequently observed over the Arctic and Nordic
13 sites of SMR, PAL and ZEP and typifies the aged and polluted aerosol distributions
14 commonly observed during the winter months in the Arctic which typify Arctic Haze. It is
15 important to note that part of the occurrence of Cluster 4 over Arctic and Nordic sites may
16 also be originating via sea spray at high wind speed (Dall'Osto et al., 2011a).

17

18 Considering again the Cluster Proximity Diagram and the position of the sites of frequent
19 occurrence in Figure 4 and Figure S5, it can be argued that the growth of nucleated
20 particles is represented by the sequence of Cluster 5 to 8 (whose maxima occur
21 sequentially at a later hour of the average day) which then feed the accumulation particles
22 represented in Cluster 9. As the modal diameter increases from 22 nm in Cluster 5
23 through Clusters 6, 7 and 8 (35 nm, 50 nm, and 60 nm) there is a tendency of the sites
24 observing these clusters to move from the coastal and Arctic sites inland reflecting the
25 aging of aerosol as it passes across the land (see Section 4). Spectra from these clusters

1 are also observed further inland at the mountain sites JFJ and ZSF. Also of interest is the
2 observation that Cluster 5 peaks in frequency in the mid-afternoon and Cluster 9 occurs
3 most during the night and morning. Clusters 5-9 and 4 are not frequently detected over
4 the belt of industrial areas of Europe where the Central European aerosol is generally
5 observed. Referring to Figure S6, Cluster 3, 5 and 4, which are frequently detected at the
6 Arctic, Nordic, Alpine and central European sites, are more frequently detected in the
7 winter months between October and March. Clusters 6, 7 and 8 (pertaining to the Nordic
8 and central European areas) show an opposite trend, peaking between April and October.

9

10 **3.3 Categorization of the Nine Clusters by Average Modal Diameters**

11 The average spectra of Clusters 1, 2, and 3 can be described as broader versions of
12 Clusters 5, 8 and 9 and are most frequently detected at one or more of the sites along the
13 belt of boundary layer sites (including IPR) where Central European aerosol is measured.
14 The broad shape of the spectra of Clusters 1-3 reflects different stages in the formation
15 and growth of the Central European particles (Figure 2a) which represent the category
16 South to North. Particle growth can be clearly seen separately in each of Cluster 1, 2 and
17 3, and by combining the colour maps into one, it is clear that they each represent a
18 different stage of a complete cycle of particle growth (see Figure S8a). As later argued,
19 these may develop in Central Europe before being detected as Arctic Haze at ZEP. In
20 comparison, the spectra within Clusters 5-9 (representing the category West to East in
21 Figure 2b) individually show less evidence of growth within each of the average 24-hour
22 colour maps, and there is a greater spread of modal diameters across the clusters.
23 However, when ordered according to modal diameter (from Cluster 5 to 9) progressive
24 growth is again seen representing particle growth as the particles move from West to East
25 across Europe albeit over a cycle much longer than for Clusters 1, 2, 3 and 4. Figure 6

1 exemplifies this further by showing how the modal diameters of the clusters grow with
2 time. These use the times of maximum particle number concentration from the colour
3 maps in Figure 4 to discern time-of-day, with additions of 24 hours to give the best fit to the
4 curve. Growth rates average 0.93 nm/h and 0.66 nm/h for the two curves, but actually
5 slow with growing particle diameter (see Figure 6). Growth rates estimated from the West
6 to East and South to North trajectories (see later) are of a similar magnitude. When
7 repeating this analysis with nucleation and accumulation mode peaks derived from curve
8 fitting to these clusters (Figures S9 and S10), it can be seen that this trend is peculiar to
9 the nucleation mode. Growth rates of the nucleation mode peak 1 are rather slower than
10 those for the mode of the full distribution seen in Figure 6. The fitted growth rates are of a
11 comparable order to those measured in situ (Kulmala et al., 2004).

12

13 Clusters 4 and 9 have the largest modal diameter amongst the sites and considering the
14 trends shown in Figure 6, tentative links can be made with particles emitted over Central
15 Europe or even sources nucleating particles detected mainly on the Atlantic coast
16 respectively. When considering the sites where each of the 9 clusters occur and the
17 likelihood in terms of the percentage occurrence at each site, a general trend can be
18 observed in that the larger the modal diameter of the cluster the greater the longitude of
19 the site it was measured at. This trend is made clear by considering the modal diameters
20 of each cluster plotted against the Longitude and Latitude weighted according to the
21 population of the cluster at each of the 24 sites (Figure 7). When carrying out this
22 analysis, trends can be observed and separated into patterns which can be grouped
23 according to whether the clusters are classified as 'fast' or 'slow' growing clusters, i.e.
24 Clusters 1 to 2 to 3 to 4 and Clusters 5 to 6 to 7 to 8 to 9 respectively. Considering
25 Clusters 5 to 9, a clear increase in modal diameter can be seen with increased Weighted

1 Longitude; this can be understood by the general movement of air masses across Europe,
2 eastwards from the Atlantic. When considering the same modal diameter plotted against
3 Weighted Latitude, the increase in modal diameter can be observed with an overall
4 decrease in Weighted Latitude, which can be understood by the bias of the strong
5 detection of Cluster 9 at FKL. In the same way that the linear and curved trends passing
6 through the modal diameters of Cluster 5 to 9 show the aging of aerosols passing from
7 West to East, Cluster 4 can be linked to the central European Clusters 1, 2 and 3. When
8 considering the modal diameters of Cluster 1 to 3 to 4, an increase can be observed again
9 with Weighted Longitude which can be understood by the movement of air masses from
10 West to East. And again when considering the modal diameters \emptyset of these same clusters
11 with Weighted Latitude, significant growth ($\Delta\emptyset = 30$ nm) is seen between Clusters 1 and 3
12 at roughly the same Weighted Latitude (Central Europe) before Cluster 4 is detected ($\Delta\emptyset =$
13 40 nm) along this sequence at a higher Weighted Latitude (corresponding to SMR, PAL
14 and ZEP).

15

16 **4. DISCUSSION**

17 While Asmi et al. (2011) sought to characterise sampling sites in terms of their particle size
18 distributions, this paper seeks to understand better the relationships between those size
19 distributions and the processes which influence them. Similar aims, but very different data
20 analyses were reported by Von Bismarck-Osten et al. (2013) in relation to measurements
21 sites in and adjacent to four European cities. For Central Europe, a principal components
22 analysis of particle number size distributions was carried out on the basis of a multiple-site
23 dataset (Costabile et al., 2009). These authors found, for the east German region,
24 statistically independent size distribution components and signature size distributions
25 similar to this work: a nucleation mode (~ cluster 1 from this work), an Aitken/aged

1 nucleation mode (~ cluster 2 from this work), a first accumulation mode (corresponding to
2 direct emissions and condensation), and a second accumulation mode resulting from
3 cloud processing.

4 Considering these sequences of clusters plotted against Weighted Longitude/Latitude, two
5 clear trends can be seen between the modal diameter of the clusters and the Weighted
6 Longitude/Latitude. The cluster results show two different aging processes leading to
7 Cluster 4 and 9 depending on whether the air masses are moving from South to North or
8 West to East.

9

- 10 • Clusters 1, 2, 3 and 4 generalise the growth of particles formed in Central Europe
11 which first age over mid-latitudes before undergoing further aging as they are
12 advected North (leading to Arctic Haze) and/or East due to the prevailing wind
13 patterns; and
- 14 • Clusters 5, 6, 7, 8 and 9 generalise a mechanism where particles age as they form at
15 coastal sites and then pass over land from West to East. They will, of course, also
16 be influenced by additional particles entering the air mass as it advects across
17 Europe.

18

19 It is envisaged that by using a higher number of clusters in this analysis additional points
20 along the purple plots (in Figures 6, 7, and S7) linking Clusters 3 and 4, would result. But
21 from these observations, a spatial generalisation can be made that at greater longitude the
22 likelihood of detecting a cluster with a large modal diameter is increased. Similar trends
23 are observed for the modal diameters measured in the equivalent volume distributions of
24 the clusters (Figure S7) except the trends for data plotted with respect to the weighted

1 longitude are straighter. These trends are examined further through case studies of
2 specific air mass trajectories (see Section 4.2).

3

4 **4.1. Influences on a Measured Particle Size Distribution**

5 Primary emissions frequently impact upon measured size distributions, especially when
6 close to source. Most notable in this context are emissions from road traffic which have an
7 immediate impact upon size distributions in the roadside environment, while advected
8 particles will also impact considerably downwind of the source. For particles in the size
9 range of less than 500 nm which are the focus of this paper, the relevant sources of
10 primary particles are generally related to combustion and include point sources as well as
11 road traffic line sources (Denier van der Gon et al. 2010). Fresh particles from road traffic
12 exhaust typically show an overall mode at around 30 nm diameter comprising the sum of
13 two modes; a mode at around 20 nm arising from nucleation of semi-volatile organic
14 compounds and a mode at around 70 nm comprising particles with a graphitic core formed
15 in the combustion chamber (Harrison et al., 2011).

16

17 Secondary nanoparticles arise from the nucleation of low-volatility materials often requiring
18 the formation of a sulphate nucleus which grows predominantly through condensation of
19 oxidised organic compounds. Many studies have reported the observation of new particles
20 formed through regional nucleation processes, starting at a few nanometres diameter and
21 growing to several tens of nanometres over a period of hours (e.g. Alam et al., 2003;
22 Kulmala et al., 2004). By plotting curves fitted through the modal diameter and maximum
23 hours of occurrence of Clusters 1, 2, 3 and 4 and Clusters 5, 6, 7, 8 and 9, a growth
24 process can be envisaged, seen in Figures 6 and S10. Given the anthropogenic origin of
25 Clusters 1, 2 and 3 in Central Europe (with traffic being the dominant source), we would

1 expect this trend to represent the growth of fresh emissions with a modal diameter of 20
2 nm.

3
4 Both primary and secondary particles can grow and shrink in size within the atmosphere.
5 Because they often comprise semi-volatile material, they are subject to condensational
6 growth in areas of high vapour concentration but may shrink by evaporation if the particles
7 move into a region of the atmosphere with low vapour concentrations such that the
8 pressure of vapour in equilibrium with the particle's surface exceeds the environmental
9 vapour pressure. The evaporation process has been clearly observed for particles
10 generated from road traffic emissions (Dall'Osto et al., 2011b). In most circumstances,
11 however, condensable vapours are continuously formed in the atmosphere through
12 oxidation processes and the net process is one of condensational growth of particles.

13
14 In addition to condensational growth, particles can grow through coagulation. However,
15 this requires relatively high number densities and at typical atmospheric concentrations
16 coagulation is likely to be a rather slow process. It is most rapid between large and very
17 small particles and consequently may impact on the number density of nanoparticles,
18 whilst having little impact on the size, and no impact on the number of larger particles.
19 While condensational growth leads to an increase in the mode of a size distribution without
20 a change in particle number concentration, coagulation will cause a growth in the mode of
21 the size distribution together with a simultaneous reduction in particle number
22 concentration.

23
24 One of the main determinants of particle number concentration, especially in proximity of
25 sources is atmospheric dilution. Particles in a plume will reduce in number concentration

1 as that plume dilutes downwind of a source or a city, with both lateral spread and vertical
2 mixing to fill the surface boundary layer. Such processes are likely to dominate over
3 deposition, although on longer timescales deposition processes can substantially influence
4 the particle number concentration and size distribution. Both wet and dry deposition
5 processes affect airborne particles and are most efficient for very small and very large
6 particles. Particles in the accumulation mode of around 100-200 nm diameter are least
7 susceptible to depositional processes and have a long atmospheric lifetime. Cloud
8 processing can also substantially impact on the number and size distribution of particles,
9 typically leading to particle growth through incorporation of vapour phase material into
10 cloud water droplets which subsequently evaporate, and also by scavenging of multiple
11 particles by single cloud water droplets.

12

13 **4.2 Air Mass Back Trajectory Case Studies**

14 The results from the cluster analysis are a static average picture of 2 years of the dataset
15 presented by Asmi et al. (2011). They give a good generalisation of how the particle
16 number distributions are grouped together across the European map. The comparison of
17 the clusters also gives an indication of the underlying processes at work as air masses
18 pass across Europe showing the aging of particles as they pass from West to East (5, 6, 7,
19 8, 9) or from South to North (category 2, Cluster 1, 2, 3, 4).

20

21 To further test the evolution of particle size distribution across Europe, and to explore the
22 processes behind their transformation, air masses passing over as many European sites
23 as possible were considered along the main West-East and North-South geographical
24 corridors formed by the EUSAAR sites. In order to do so, we present four case studies of
25 four different air mass trajectories: case study 1 (MHD to FNK, West to East, Figure 8),

1 case study 2 (KPO to MHD, East to West, Figure 9), case study 3 (JFJ-HPB to ZEP, South
2 to North, Figure 10) and case study 4 (PAL to CMN, North to South, Figure 11). Each
3 trajectory (calculated by the British Atmospheric Data Centre (BADC) Trajectory Service) is
4 plotted onto a particle number emission (PN) map (Denier van der Gon et al, 2010) ($\varnothing \leq$
5 300 nm on a 7 x 7 km grid) in order to indicate the level of emission activity along the
6 trajectory. The transit time between the monitoring sites was estimated and the particle
7 size spectra at each monitoring site at the relevant trajectory time (1 ± 1 hour, total 3 hours)
8 were extracted from the dataset. Each of the Figures 8-11 has the same structure: (a) the
9 wind rose direction studied; (b) the 5-day air mass back trajectories; (c) the monitoring
10 site-specific size resolved particle number concentration averages; (d) the nucleation,
11 Aitken and accumulation modes (in number concentration) of each monitoring site,
12 obtained from the fitting of log normal modes to (c); (e) the monitoring site-specific size
13 resolved particle volume concentration averages; (f) the volume concentration of the
14 accumulation, Aitken and accumulation modes of each monitoring site, obtained from the
15 fitting log modes of (e). The modes were fitted to the number and volume distributions
16 using the multi-peak fitting package in Igor Pro 6.34A. Peaks were manually added and
17 positioned until the optimum fit was achieved when the algorithm was run.

18

19 The resulting modal diameters are indicated by the grey dots on the spectrum stacks and
20 areas under these fitted modes were plotted against distance from the site where the first
21 recordable spectrum was measured. The dotted lines in Figures 8-11(c,e) represent a
22 tentative linkage indicative of possible evolution of particle modes along the trajectory. In
23 the next four sub-sections, details of each of the four case studies are presented.

24

25 **4.2.1 Case Study 1: West to East Trajectory**

1 Figure 8 shows an air mass trajectory started on 18th December 2008 off the West coast
2 of the Republic of Ireland over the Atlantic Ocean in an area of frontal activity. A high
3 percentage of cloud and rain accompanied the air mass as it passed over MHD and HWL
4 (Figure S11 and S12). As the air mass passed from CBW to KPO between the 21st and
5 22nd of December 2008, the synoptic charts for these two days indicate that the air mass
6 trajectory passed between a region of high pressure, centred over France and a region of
7 low pressure positioned over the Nordic countries (Figure S11 and S12). Between these
8 two regions of pressure two weather fronts stretched across the UK, along the path of the
9 trajectory and into Eastern Europe. Again, rain and cloud was present along the trajectory
10 from CBW to OBK. The persistent rain and cloud is responsible for extensive aerosol
11 deposition from the air mass.

12

13 From CBW to KPO the atmospheric pressure dropped from 1020 mb to a minimum of 980
14 mb at MPZ before rising again towards 1020 mb at KPO. This low pressure was
15 accompanied by between 80 and 100% cloud cover which then reduced to between zero
16 and 40% after KPO. The high cloud cover is also reflected in the low downward short
17 wave radiation flux (DSWF) reaching a maximum of 50 W/m^2 during the day time, rising to
18 200 and 350 W/m^2 after the air mass passes KPO. The Planetary Boundary Layer Height
19 (PBLH) also kept to a low value of $\sim 500 \text{ m}$ towards MPZ after which a diurnal cycle was
20 re-established due to the clearer skies. After KPO, the PBLH reached a maximum of 1.7
21 km. Rainfall was reported along the trajectory from CBW to MPZ (Figure S11, S12).

22 Overall, the meteorology along this trajectory was wet and cloudy up to the point when the
23 air mass arrived at MPZ, when the weather pattern started to change to a situation where
24 high pressure sat over the measurements sites on 23rd and 24th December. Up until this
25 point the downward solar flux was low due to the heavy cloud cover, which in turn led to a

1 low boundary layer height. Regional nucleation would be very unfavoured under these
2 conditions. In fact, precipitation scavenging explains the relatively low particle number
3 concentrations accompanied by a strong accumulation mode due to the less efficient
4 precipitation scavenging of this size range. Since the air mass originated over the Atlantic,
5 a strong sea salt source (coarse mode indicated in the volume spectrum, Figure 8e) would
6 be expected to contribute to the initial spectrum recorded at MHD. For this trajectory,
7 hourly spectra were not available at HWL and FKL within the ± 1 hour window used to
8 select spectra and in order to have some representation, a ± 120 hour window was used to
9 generate spectra. Even so, within this compromise, the development of the particle size
10 spectrum can be seen as a mode at 40 nm is observed at MHD and HWL which then
11 grows to 50 nm at CBW corresponding to Cluster 7, having its highest frequency of
12 detection. The hugely increased number concentration at CBW implies that direct
13 emissions must be largely responsible. As noted in the previous section, this may be
14 largely the result of road traffic emissions. The modal diameter then increased from 50 nm
15 at CBW to 70 nm at MPZ (indeed moving from Cluster 5 type to Cluster 8-type, Figure 4,
16 5). There are two other modes which appeared along the trajectory with a lower and
17 higher diameter, the larger of which contributed to the final spectrum causing Cluster 9-
18 type spectra characteristic of FKL. In other words, this case study 1 is very well described
19 by the Cluster-Proximity Diagram (Figure 5), where the particle spectrum type moved from
20 left to right across the bottom of the diagram from Cluster 5 to Cluster 9 showing the
21 influence of aerosol aging and fresh emissions.

22

23 The air mass started with a total particle count just less than 1000 cm^{-3} at MHD and then
24 grew significantly through 4000 cm^{-3} at HWL to a maximum of $12,000 \text{ cm}^{-3}$ at CBW. The
25 mode common to MHD, HWL and CBW grew significantly after HWL, at which the main

1 contribution was to a mode at 80 nm. As the air mass passed over BOS, WAL and MPZ,
2 the total number of particles cm^{-3} counted stayed under 4,000 until MPZ after which it fell
3 to below 1,000 cm^{-3} (Figure 8 c, d). With regards to the volume, this steadily increased
4 due to one mode at just below 0.2 μm at HWL which developed right up until MPZ after
5 which there was a staggered fall as the air mass approached FKL (Figure 8 e, f). It is also
6 worth pointing out that between CBW and KPO, where this size mode was observed: (i)
7 there was almost 100% cloud cover, precipitation was present and the RH approached
8 100% favouring aqueous phase processing, and (ii) there were substantial anthropogenic
9 emissions of particles and gases. After KPO, the RH steadily decreased together with the
10 contribution to the total volume from these two condensation modes. Interestingly, a
11 second mode was seen to appear at just below 0.2 μm at WAL which then also started to
12 grow as the air mass passed over MPZ, OBK, KPO before arriving at FKL. The growth of
13 these two modes within overlapping time frames (both at a rate of $1.2 \mu\text{m}^3 \text{cm}^{-3} \text{h}^{-1}$)
14 explains why there was maximum volume observed at MPZ. After MPZ the total volume
15 concentration fell, presumably due to deposition.

16

17 **4.2.2 Case Study 2: East to West Trajectory**

18 Whereas the West-to-East trajectory considered a case in the winter, the East-to-West
19 trajectory case study was taken during the spring (11th-16th April 2009; Figure 9). At the
20 start of the trajectory (11th April 2009), the air mass originated in a region of low pressure
21 over Eastern Europe with a slack pressure gradient and stagnated air which resulted in it
22 taking 48 hours for the air mass to drift from KPO to MPZ (Figure S13 and S14). A large
23 nucleation mode measured at KPO was washed out by a period of rain starting shortly
24 after the air mass left KPO and headed to MPZ, after which the air mass experienced no
25 rain, with an RH of $\sim 80\%$ and temperature of $5\text{-}10^\circ\text{C}$. Once past MPZ, the air pressure

1 increased (> 1000 mb) until it passed over the UK where it dipped twice down to 980 mb
2 between CBW and HWL and HWL and MHD. The DSWF showed a typical diurnal pattern
3 reaching a maximum of 600-700 W/m² during the day which was modulated by the
4 presence of cloud at around 40% over MPZ, WAL, CBW and as high as 80% over HWL.
5 This sequence of washout followed by clearer skies promoted the nucleation and growth of
6 particles seen in the number spectra. The baseline of PBLH rose from ~100 m at KPO to
7 1000 m at MHD, peaking during the day at its highest value of 1.5 km at MPZ (Figure S13
8 and S14). As the air mass approached MHD (16th April 2009), the cloud cover reached
9 100% and was accompanied by rain as it coincided with a cold weather front between a
10 low in the south and a high in the north of Great Britain.

11

12 The two particle spectra collected at KPO and MPZ were classified as of Cluster 1-type
13 before developing into Cluster 2-type spectra at WAL, and finally ending as Cluster 3-type
14 spectrum at MHD. Whilst this structure begins and ends as category 1 clustering type, the
15 intermediate monitoring site at CBW and HWL presented a Cluster 8-type structure. In
16 other words, this sequence of cluster classifications does not follow an intuitive trend (even
17 across the Cluster-Proximity Diagram). Also, because of the relatively dry conditions
18 compared to the previous West-to-East scenario, nucleation peaks were detected with the
19 stagnating air mass which progressively decreased in number density when approaching
20 MHD. MPZ was the first site free of rain, and showed a multi-modal distribution. There
21 was a considerable loss in volume from MPZ to WAL and CBW associated with a
22 reduction in the accumulation mode, but growth of a nucleation mode was seen. This
23 however was lost at HWL but grew in again at MHD. Local sources including nucleation
24 and deposition processes appear to be the dominant factor for this trajectory. In summary,
25 from the East to West Trajectory case study 2 (Figure 9), it is clear that it is more difficult to

1 develop a mechanistic interpretation of the development of the particle number and
2 volume spectra than for the West to East Trajectory Case Study 2 (Figure 8). This may be
3 due to the greater complexity in the initial aerosol composition over land compared to the
4 relatively clean air originating over the Atlantic Ocean.

5 **4.2.3 Case Study 3: South to North Trajectory**

6 Case studies 1 and 2 considered air mass back trajectories moving at relatively constant
7 latitude across the European continent. In contrast, case studies 3 and 4 are based upon
8 air mass back trajectories moving at relatively constant longitude across the European
9 continent. In case study 3, the air mass moved from land to sea, but this time arriving at
10 the Arctic site of Zeppelin (ZEP) and starting from the relatively clean air sites of JFJ and
11 HPB (typified by Cluster 7, see Figures 10).

12

13 The synoptic maps for the beginning of February 2008 show a persistent weather system
14 with low pressure over the UK and high pressure over Eastern Europe causing the air
15 mass considered in our trajectory to travel up from HPB to ZEP crossing a cold and
16 cold/warm weather front as the air mass approached ZEP (Figure S15 and S16). Most
17 noticeable in the meteorology was the presence of snow and rain as the trajectory passed
18 between SMR and ZEP. This was reflected in the temperature profile as the value fell
19 below 0°C between ASP and ZEP which otherwise rose to a maximum of around 5°C.
20 The cloud cover along the trajectory was high, dipping away from 100% and the DSWF
21 reached a maximum of ~ 300 W/m² during the day at the start of the trajectory and
22 progressively became weaker over the 5 days. The PBLH varied between ~ 600 m before
23 climbing to 1400 m half way between SMR and ZEP.

24

1 The final particle size spectrum at ZEP was typical of the characteristic average spectrum
2 measured at this site, described by Cluster 4, which has the largest modal diameter of
3 between 100 nm and 150 nm. For the scenario considered in Figure 10, the first site was
4 JFJ and was relatively clean, being located at top of the Jungfrauoch above the boundary
5 layer pollution. The second site on the trajectory was at MPZ and both the total particle
6 number and volume were much higher at this boundary layer site. The modal diameters of
7 30 nm and 100 nm probably represented traffic aerosol and secondary particles
8 respectively. As the air mass travelled north towards ZEP, fewer particle sources were
9 encountered (see Figure 10) and the particle number decreased to values comparable
10 with the initial number at JFJ. Steady growth of modal diameters occurred with the
11 nucleation mode at MPZ apparently transitioning to an accumulation mode at ZEP.

12

13 When comparing this case study with the cluster classification (Figure 5), the spectra
14 followed from left to right across the Cluster Proximity Diagram from a Cluster 1 spectrum
15 at MPZ, to a Cluster 2 spectrum at VHL, which then becomes successively a Cluster 3 and
16 Cluster 4 spectrum at SMR and ZEP, respectively. In other words, the South-to-North
17 trajectories were generalised by the upper left-to-right nodal positions in the Cluster-
18 Proximity Diagram. In summary, case study 3 well represents the second category of our
19 study (South to North, Cluster 1, 2, 3 and 4). We do not include JFJ in the latter
20 description, as it clearly experienced a different (free troposphere) air mass to MPZ.

21

22 **4.2.4 North to South Trajectory**

23 For the North-to-South trajectory case study, trajectories were selected which passed
24 through the Nordic countries, across central Europe to CMN. The chosen trajectory
25 arrived at CMN on the 17th October 2009 (Figure 11). The air mass encountered mainly

1 cloudy conditions and the spectra appeared more representative of local sources due to
2 the quicker removal times at lower particle sizes (< 50 nm). Throughout the five-day
3 duration of the trajectory path (11th-17th October 2009), the synoptic charts showed a high
4 pressure centred over the southern UK with low pressure in Eastern Europe. The
5 trajectory began at the PAL monitoring site (11th October 2009), moved quickly over MPZ
6 during the first two days and took a further 3 days to pass by HPB, ZSF before finally
7 arriving at CMN. The cloud cover remained high (90-100%) along the trajectory, falling
8 towards 0-20% between SMR and ASP (Figures S17-S18). However, the diurnal patterns
9 of the DSWF were distinct, reaching a maximum of 400 W/m² in the daytime. There were
10 patches of rain along the trajectory between ASP and WAL and between ZSF and CMN
11 due to a weather front. As to be expected, the temperature increased from -10°C at PAL to
12 a daytime high of 20°C at CMN and the RH dropped from 100% to between 40 and 60 %
13 at CMN (Figures S17-S18). It should be noted that the final three stations are all sited at
14 high altitude, which will have influenced the data (HPB 988 m; ZSF 2670 m and CMN
15 2165 m a.s.l.)

16

17 When classifying these, it is interesting that bimodal distributions are observed which are
18 not clearly identified as belonging to any of our clusters until considering the lower
19 percentile of the distributions, e.g. ZSF, HBP, CMN, all belong to Cluster 2 identified by the
20 lower percentile distributions (see Figure S19). The remaining spectra are assigned as
21 follows: PAL Cluster 3; SMR Cluster 6; and WAL and CMN Cluster 1. In this classification,
22 there is no discernible trend across the Cluster-Proximity Diagram, although it can be seen
23 that two modes are detected at PAL at 30 nm and 200 nm which are possibly due to a
24 previous Arctic Haze event. In other words, whilst case study 3 (South to North) well
25 described the second aerosol clustering category, the current case study 4 (North to

1 South) does not. Differences in the trend in number and volume concentrations along the
2 trajectory are striking (Figure 11). Both start low, but while particle volume (Figure 11e)
3 shows a broadly upward trend with distance (falling slightly at ZSF), particle number peaks
4 (Figure 11c) sharply at WAL and MPZ and then declines steadily. These appear to be
5 large injections of fresh primary particles in the vicinity of WAL and MPZ which
6 subsequently decrease with ageing, while these and gas-to-particle conversion lead to a
7 steady increase in accumulation mode particles (Figure 11 e). By the time the air mass
8 reaches CMN (17th October 2009, Figure 11), a third mode at 20 nm is observed. The
9 equivalent volume distribution shows a consistent and persistent mode at 200 nm which
10 remains but grows in volume throughout the course of the trajectory.

11

12 **5. CONCLUSIONS**

13 Two years of harmonised-daily EUSAAR number size distribution data collected and
14 averaged from 24 European field monitoring sites have been analysed using *k*-means
15 cluster analysis. The results generalise the European near surface aerosol particle size
16 distributions and show to what extent neighbouring sites share common size distributions.
17 These characteristics give insights into the aerosol processes at work and the likelihood of
18 their occurrence. Rather than being restricted to specific areas, as would be expected
19 considering the characteristic average shapes of particle spectra at the various sites (Asmi
20 et al., 2011), the clusters all have a likelihood of being detected at a large proportion of the
21 sites. In general, a central vs outer Europe divide was observed when considering the
22 median to upper quartiles of the frequency of detection at each site and when merged into
23 two groups, nucleation and growth of particles can be observed on two time scales. The
24 clusters detected most frequently within the Central European region - in and around
25 Germany where the spatial density of emissions is anticipated to be high - had less

1 seasonal dependence and much broader nucleation and accumulation modes reflecting
2 the increased likelihood of more diverse emission sources from anthropogenic emissions
3 mixing into an air mass. At the higher number concentrations, these merge into a
4 continuous curve with a single modal diameter whereas at lower concentrations, a bimodal
5 distribution was present which accounted for the lower likelihood of these cluster types
6 being detected at extreme locations at the Nordic, Alpine and Arctic sites. In particular, the
7 diurnal trends in the spectra showed strong evidence of afternoon growth of nucleated
8 particles within these Central European clusters. In contrast, the remaining 6 outer-
9 European clusters did not show as fast a development in the nucleation and growth of
10 particles on a regular diurnal scale but instead collectively showed a modal diameter
11 dependence on the longitude (from West to East) of the site at which they were most likely
12 to be detected. Nucleation-type clusters (< 20 nm) were most likely to be observed at the
13 sites close to the Atlantic Coast and as the modal diameter shifted from cluster to cluster,
14 the most frequent site of detection moved across Europe to the distant sites in the
15 Mediterranean and Arctic regions where the modal diameter was greater than $0.1 \mu\text{m}$.
16 This effect is most strikingly seen when the modal diameters of the clustered spectra are
17 plotted against the longitude of the sites where they were detected, weighted by the
18 population of each cluster at the sites. A similar effect could be seen for the Central-
19 European clusters which when linked with weighted Latitude suggested a South-to-North
20 transport and development of aerosol released in Central-Europe (with a modal-diameter
21 of ~ 45 nm) leading to Arctic Haze (modal diameter ~ 150 nm) over three days. There also
22 may be contributions from aerosol arising from the Saharan region, e.g. at ZSF where the
23 most frequent and significant transport of aerosols originates from Africa.

24

1 When considering the case studies of West to East and South to North air masses
2 (Figures 8 and 10) we can infer a growth rate. For the West to East case study, the modal
3 diameter of the particles passing from HWL to MPZ grows at a rate of $\sim 2.9 \text{ nm h}^{-1}$. This is
4 double the growth rate of the modal diameter of the particles in the air mass travelling
5 North from MPZ to ZEP which is calculated to be 1.3 nm h^{-1} . These values are within the
6 range of the values reviewed by Kulmala et al. (2004) who reported particle growth rates
7 between 1 and 20 nm h^{-1} , with exceptions of some estimates in coastal areas giving
8 growth rates as high as 200 nm h^{-1} and the smallest reported growth rates around 0.1
9 nm/h observed in clean polar areas. A more recent study (Vaananen et al., 2013) has also
10 shown very slow growth rates in Northern Scandinavia ($< 1 \text{ nm/h}$).

11

12 In summary, when considering the particle size spectra observed at each of the sites over
13 which trajectories pass along the North-South and West-East axes of the EUSAAR sites,
14 evidence of particle growth is observed. Case studies, which consider the movement of
15 the air masses along the North-to-South and East-to-West axes of the EUSAAR sites,
16 show much greater complexity, largely due to a more aged aerosol being present at the
17 trajectory starting point. The two clear trends based on West-to-East and South-to-North
18 air mass movement can be distinguished as belonging to two particle growth mechanisms:

- 19 1. The West-to-East particle development can be best seen in the volume spectrum as
20 two volume modes within overlapping time frames which are seen to start with a
21 modal diameter just below $0.2 \mu\text{m}$, and are observed to grow to $0.7 \mu\text{m}$ and increase
22 in volume at a rate of $1.2 \mu\text{m}^3 \text{ cm}^{-3} \text{ h}^{-1}$.
- 23 2. The South-to-North trajectory particle development is best seen in the number
24 spectra originating at JFJ. This clean air mass is fed with anthropogenic emissions
25 before arriving at MPZ where it has a strong number mode at 40 nm . The total

1 number of particles is highest at MPZ and then steadily decreases as the air mass
2 tracks North, and on its journey, the mode at 40 nm grows in modal diameter to ~ 150
3 nm (Arctic Haze).

4
5 Although these four case studies illustrate the key processes affecting the aerosol as air
6 masses advect across Europe, they present only snapshots of behaviour which is strongly
7 influenced by the prevailing meteorology and hence local conditions at the time of
8 sampling. They do, however, serve to illustrate that the general trends expressed in the
9 Cluster Proximity Diagram (Figure 5) are observable in individual pan-European
10 trajectories, as well as representing longer-term process averages. This study strongly
11 suggests that the evolution of ultrafine and fine particles is heavily dominated by
12 condensation processes, further demonstrating the remarkable dynamics of particles in the
13 atmosphere.

14 15 **ACKNOWLEDGEMENTS**

16 The National Centre for Atmospheric Science is funded by the U.K. Natural Environment
17 Research Council. This work was also supported by the European Union EUCAARI
18 (Contract Ref. 036833) and EUSAAR (Contract Ref. 026140) research projects. Thanks
19 are also expressed to the British Atmospheric Data Centre, which is part of the NERC
20 National Centre for Atmospheric Science (NCAS), for providing access to calculated
21 trajectories using data from the European Centre for Medium Range Weather Forecasts.

22
23 Acknowledgements for the funding of data collection and harmonisation appear in Asmi et
24 al. (2011) and in the interests of brevity are not repeated here.

1 REFERENCES

- 2
3 Alam, A., Shi, J. P. and Harrison, R. M.: Observations of new particle formation in urban
4 air, *J. Geophys. Res.*, 108, 4093-4107, 2003.
5
6 Asmi A., Wiedensohler A., Paj P., Fjaeraa A. - M., Sellegri K., Birmili W., Weingartner E.,
7 Baltensperger U., Zdimal V., Zikova N., Putaud J. - P., Marinoni A., Tunved P., Hansson
8 H. - C., Fiebig M., Kivekäs N., Lihavainen H., Asmi E., Ulevicius V., Aalto P. P., Swietlicki
9 E., Kristensson A., Mihalopoulos N., Kalivitis N., Kalapov I., Kiss G., Leeuw G. de, Henzing
10 B., Harrison R. M., Beddows D., O'Dowd C., Jennings S. G., Flentje H., Weinhold K.,
11 Meinhardt F., Ries L. and Kulmala M.: Number size distributions and seasonality of
12 submicron particles in Europe 2008–2009, *Atmos. Chem. Phys.*, 11, 5505-5538, 2011.
13
14 Beddows, D. C. S., Dall'Osto, M. and Harrison, R. M.: Cluster Analysis of Rural, Urban
15 and Curbside Atmospheric Particle Size Data, *Environ. Sci. Technol.*, 43, 4694-4700,
16 2009.
17
18 Birmili, W., Weinhold, K., Nordmann, S., Wiedensohler, A., Spindler, G., Müller, K.,
19 Herrmann, H., Gnauk, T., Pitz, M., Cyrys, J., Flentje, H., Nickel, C., Kulhbusch, T., Lschau,
20 G., Haase, D., Meinhardt, F., Schwerin, A., Ries, L. and Wirtz, K.: Atmospheric aerosol
21 measurements in the German Ultrafine Aerosol Network (GUAN), – Part 1: Soot and
22 particle number distributions, *Gefahrst. Reinhalt. L.*, 69, 137-145, 2009.
23
24 Boulon J. , Sellegri, K., Venzac, H. , Picard, D., Weingartner, E., Wehrle, G.,
25 Collaud Coen, M., Bütkofer, R., Flückiger, E., Baltensperger, U. and Laj, P.: New particle
26 formation and ultrafine charged aerosol climatology at a high altitude site in the Alps
27 (Jungfrauoch, 3580 m a.s.l., Switzerland), *Atmos. Chem. Phys.*, 10, 9333-9349, 2010.
28
29 Boulon J., Sellegri, K., Hervo, M., Picard, D., Pichon, J.-M., Freville, P. and Laj, P.:
30 Investigation of nucleation events vertical extent: a long term study at two different altitude
31 sites, *Atmos. Chem. Phys.*, 11, 5625-5639, 2011
32
33 Central Intelligence Agency: The World Factbook 2009, Central Intelligence Agency,
34 Washington, DC, USA, 2009.
35
36 Charron, A. and Harrison, R. M.: Primary particle formation from vehicle emissions during
37 exhaust dilution in the roadside atmosphere, *Atmos. Environ.*, 37, 4109-4119, 2003.
38
39 Charron, A., Birmili, W. and Harrison, R. M.: Factors influencing new particle formation at
40 the rural site, Harwell, United Kingdom, *J. Geophys. Res.*, 112, 4210, 2007,
41 doi:10.1029/2007JD008425.
42
43 Costabile, F., Birmili, W., Klose, S., Tuch, T., Wehner, B., Wiedensohler, A., Franck, U.,
44 König, K., and Sonntag, A.: Spatio-temporal variability and principal components of the
45 particle number size distribution in an urban atmosphere, *Atmos. Chem. Phys.*, 9, 3163-
46 3195, 2009.
47

1 Dall'Osto, M., Monahan, C., Greaney R., Beddows, D. C. S., Harrison, R. M., Ceburnis, D.
2 and O'Dowd, C. D.: A statistical analysis of North East Atlantic (submicron) aerosol size
3 distributions, *Atmos. Chem. Phys.*, 11, 12567-12578, 2011a.
4 Dall'Osto, M., Thorpe, A., Beddows, D. C. S., Harrison, R. M., Barlow, J. F., Dunbar, T.,
5 Williams, P. I. and Coe, H.: Remarkable dynamics of nanoparticles in the urban
6 atmosphere, *Atmos. Chem. Phys.*, 11, 6623-663, 2011b.
7
8 Denier van der Gon, H., Visschedijk, A., Johansson, C., Ntziachristos, L. and Harrison, R. M.:
9 Size-resolved pan-European anthropogenic particle number inventory , paper presented at
10 International Aerosol conference (oral), 29/8-3/9 2010, Helsinki, 2010.
11
12 EEA CSI 004-Exceedance of air quality limit values in urban areas (version 2), available
13 at: [http://themes.eea.europa.eu/IMS/IMS/lprecis/lprecifkcation20080701123452/](http://themes.eea.europa.eu/IMS/IMS/lprecis/lprecifkcation20080701123452/lAssessment1243521792257/viewcontent)
14 [lAssessment1243521792257/viewcontent](http://themes.eea.europa.eu/IMS/IMS/lprecis/lprecifkcation20080701123452/lAssessment1243521792257/viewcontent) (last access: November 2012), 2009.
15
16 Eleftheriadis, K., Colbeck, I., Housiadas, C., Lazaridis, M., Mihalopoulos, N., Mitsakou, C.,
17 Smolík, J. and Ždímal V.: Size distribution, composition and origin of the submicron
18 aerosol in the marine boundary layer during the eastern Mediterranean "SUB-AERO"
19 experiment, *Atmos. Environ.*, 40, 6245-6260, 2006.
20
21 Harrison, R. M, Beddows, D. C. S. and Dall'Osto, M.: PMF analysis of wide-range particle
22 size spectra collected on a major highway, *Environ. Sci. Technol.*, 5522-5528, 2011.
23
24 Harrison, R. M. and Jones, A. M.: Multisite study of particle number concentrations in
25 urban air, *Environ. Sci. Technol.*, 39, 6063-6070, 2005.
26
27 Hartigan, J. A. and Wong, M. A.: A *k*-means clustering algorithm., *App. Statist.*, 28,100–
28 108, 1979.
29
30 Hildebrandt, L., Engelhart, G. J., Mohr, C., Kostenidou, E., Lanz, V. A., Bougiatioti, A.,
31 DeCarlo, P. F., Prevot, A. S. H., Baltensperger, U., Mihalopoulos, N., Donahue, N. M. and
32 Pandis, S. N.: Aged organic aerosol in the Eastern Mediterranean: the Finokalia Aerosol
33 Measurement Experiment – 2008, *Atmos. Chem. Phys.*, 10, 4167-4186, 2010.
34
35 Kopanakis, I., Chatoutsidou, S.E., Torseth, K., Glytsos, T. and Lazaridis, M.: Particle
36 number size distribution in the eastern Mediterranean: Formation and growth rates of
37 ultrafine airborne atmospheric particles, *Atmos. Environ.*, 77, 790-802, 2013.
38
39 Kulmala, M., Vehkamäki, H., Petaäjä , T., Dal Maso, M., Lauri, A., Kerminen, V.-M., Birmili,
40 W., and McMurry, P. H.: Formation and growth rates of ultrafine atmospheric particles: A
41 review of observations, *J. Aerosol Sci.*, 35, 143–176, 2004.
42
43 Philippin, S., Laj, P. and Putaud, J.-P., Wiedensohler, A., de Leeuw, G., Fjaeraa, A., Platt,
44 U., Baltensperger, U. and Fiebig, M.: EUSAAR An Unprecedented Network of Aerosol
45 Observation in Europe, *Eurozoru Kenkyu*, 24, 78–83, 2009.
46
47 R Development Core Team. R: A language and environment for statistical computing. R
48 Foundation for Statistical Computing, Vienna, Austria. ISBN 3-900051-07-0, URL
49 <http://www.R-project.org/>, 2011.
50

1 Reddington, C. L., Carslaw, K. S., Spracklen, D. V., Frontoso, M. G., Collins, L.,
2 Merikanto, J., Minikin, A., Hamburger, T., Coe, H., Kulmala, M., Aalto, P., Flentje, H.,
3 Plass-Dülmer, C., Birmili, W., Wiedensohler, A., Wehner, B., Tuch, T., Sonntag, A.,
4 O'Dowd, C. D., Jennings, S. G., Dupuy, R., Baltensperger, U., Weingartner, E., Hansson,
5 H.-C., Tunved, P., Laj, P., Sellegri, K., Boulon, J., Putaud, J.-P., Gruening, C.,
6 Swietlicki, E., Roldin, P., Henzing, J. S., Moerman, M., Mihalopoulos, N., Kouvarakis,
7 G., Ždímal, V., Zíková, N., Marinoni, A., Bonasoni, P. and Duchi, R.: Primary versus
8 secondary contributions to particle number concentrations in the European boundary layer,
9 *Atmos. Chem. Phys.*, 11, 12007-12036, 2011.

10

11 Ström, J., Umegard, J., Torseth, K., Tunved, P., Hansson, H.-C., Holmen, K., Wismann,
12 V., Herber, A. and König-Langlo, G.: One year of particle size distribution and aerosol
13 chemical composition measurements at the Zeppelin Station, Svalbard, March 2000-
14 March 2001, *Phys. Chem. Earth*, 28, 1181-1190, 2003.

15

16 Tunved, P., Ström, J. and Krejci, R.: Arctic aerosol life cycle: linking aerosol size
17 distributions observed between 2000 and 2010 with air mass transport and precipitation at
18 Zeppelin station, Ny-Ålesund, Svalbard, *Atmos. Chem. Phys. Discuss.*, 12, 29967-30019,
19 2012.

20

21 Venzac, H., Sellegri, K., Laj, P., Villani, P., Bonasoni, P., Marinoni, A., Cristofanelli, P.,
22 Calzolari, F., Fuzzi, S., Decesari, S., Facchini, M.-C., Vuillermoz, E. and Verza, G. P.:
23 High frequency new particle formation in the Himalayas, *PNAS*, Vol. 105, 15666-15671,
24 2008.

25

26 Vaananen, R., Kyro, E.-M., Nieminen, T., Kivekas, N., Junninen, H., Virkkula, A., Dal
27 Maso, M., Lihavainen, H., Viisanen, Y., Svenningsson, B., Holst, T., Arneth, A., Aalto, P.
28 P., Kulmala, N. and Kerminen, V.-M.: Analysis of particle size distribution changes
29 between three measurement sites in Northern Scandinavia, *Atmos. Chem. Phys. Discuss.*,
30 13, 9401-9442, 2013.

31

32 Von Bismarck-Osten, C., Birmili, B., Ketzler, M., Massling, A., Petaja, T. and Weber, S.:
33 Characterization of parameters influencing the spatio-temporal variability of urban particle
34 number size distributions in four European cities, *Atmos. Environ.*, 77, 415-429, 2013.

35

36 Wiedensohler, A., Birmili, W., Nowak, A., Sonntag, A., Weinhold, K., Merkel, M., Wehner,
37 B., Tuch, T., Pfeifer, S., Fiebig, M., Fjaraa, A. M., Asmi, E., Sellegri, K., Depuy, R.,
38 Venzac, H., Villani, P., Laj, P., Aalto, P., Ogren, J. A., Swietlicki, E., Williams, P., Roldin,
39 P., Quincey, P., Hüglin, C., Fierz-Schmidhauser, R., Gysel, M., Weingartner, E.,
40 Riccobono, F., Santos, S., Gruning, C., Faloon, K., Beddows, D., Harrison, R. M.,
41 Monahan, C., Jennings, S. G., O'Dowd, C. D., Marinoni, A., Horn, H.-G., Keck, L., Jiang,
42 J., Scheckman, J., McMurry, P. H., Deng, Z., Zhao, C. S., Moerman, M., Henzing, B., de
43 Leeuw, G., Loschau, G. and Bastian S.: Mobility particle size spectrometers:
44 harmonization of technical standards and data structure to facilitate high quality long-term
45 observations of atmospheric particle number size distributions, *Atmos. Meas. Tech.*, 5,
46 657-685, 2012.

47

48 Zhang, T., Ramakrishnan, R. and Livny, M.: BIRCH: A New Data Clustering Algorithm and
49 Its Applications", *Data Mining and Knowledge Discovery*, 1, 141-182, 1997.

50

1
2
3
4
5
6
7
8
9
10
11
12
13
14
15
16
17
18
19
20
21
22
23
24
25
26
27
28
29
30
31
32
33
34
35
36
37
38
39
40
41
42
43
44
45
46

TABLE LEGENDS:

Table 1. Locations and names of stations used in the data analysis. The site altitudes are given in reference to standard sea level. The areas are grouped by European sub-divisions using definitions from Central Intelligence Agency (2009). Country codes are given in the ISO 3166 standard.

FIGURE LEGENDS

Figure 1. Location of the 24 EUSAAR and GUAN stations in Table 1.

Figure 2. Average Cluster Spectra resulting from the cluster analysis of the daily mean spectra collected at each of the 24 EUSAAR sites. (a) Clusters 1, 2 and 3 are the broad central European spectra and the Arctic spectrum 4 and (b) Clusters 5, 6, 7, 8 and 9 are the narrower size distributions observed at sites outside of the central European area.

Figure 3. Frequency of the clusters measured at each of the sites arranged in columns of similar patterns.

Figure 4. Average clustered particle size distributions (*cluster 1-9 left hand panels*) and the spatial distribution of each cluster (*centre panels*). The solid black line shows the average spectrum and the dashed lines show the 10th, 25th, 75th and 90th percentile spectrum. The maximum and minimum spectra are traced out by the extremities of the shaded areas. The middle panels show where each of the clusters are most likely to be detected. When counting the spectrum types within the whole data set, the sites which collected above the 90th, 75th and 50th percentile were marked with a progressively lighter orange colour (see Figure S5 for the frequency distributions). Circles denote boundary layer sites and triangles denotes sites of relatively high altitude. The right hand panel shows the colour maps plotted using the average day of hourly spectra for each of the clusters. [The shade from red-yellow-whites represent a linear scale of $dN / d\log(D_p)$ between the minimum value of the 10th percentile spectrum and the maximum value of the 90th percentile spectrum shown for each cluster.]

Figure 5. Cluster Proximity Diagram. Each node in the diagram represents a cluster and each cluster is arranged according to its similarity to its neighbour. The modal diameter increases from left to right across the diagram and the two shaded regions indicate those clusters which are most frequently detected in central Europe (dark grey) and those which are not (lighter shades of grey).

1 The times positioned next to each node indicate when the maximum particle
2 number concentration of each cluster occurred.
3
4

5 **Figure 6.** Plot showing how the modal diameters MD of the average cluster spectra vary
6 with the hour HR of their maximum particle number concentration [PN]. The
7 purple (1,2,3 and 4) and blue (5,6,7,8 and 9) colours depict two aggregated
8 trends observed in the data based on a South to North and West to East air
9 mass movement. The rates of growth from cluster to cluster are: for the
10 purple (1, 2, 3 and 4) 0.9, 0.9 and 1.0 nm / hr; and for the blue (5, 6, 7, 8 and 9)
11 equal 0.59, 0.55, 0.82 and 0.67 nm / hr [Fitted lines: $y = 0.96x + 12.8$ and
12 $y = 0.67x + 8.11$]
13

14 **Figure 7.** Using the number distribution, the fitted modal diameter of each cluster (1-9)
15 is plotted against the Weighted Longitude or Latitude, calculated for each
16 cluster, using $WL = \sum_i^{24} W_i \cdot X_i / \sum_i^{24} W_i$, where X_i is the latitude/longitude of the
17 sites where the cluster is detected and W_i is the corresponding population of
18 the cluster across the 24 sites.
19

20 **Figure 8.** CASE STUDY 1 (West to East) Temporal development of the particle size
21 spectra plotted along the 5 day back trajectory shown in plotted green/red
22 from midnight to midnight on the particle number (PN) emission map shown
23 in panel (b), starting southwest of MHD on 18th December 2008 and arriving
24 at FKL on 24th December 2008 at 0:00. The stacked number and volume
25 spectra (c, e) show the size distributions measured at the sites as the air
26 mass passes. The modal diameter of the fitted distributions are indicated by
27 circles and the progress plotted by the coloured lines which are coded to
28 indicate the fraction of total number for each site plotted against distance in
29 the right hand panels (d, f). The dotted lines in panels (c) and (e) are
30 primarily to guide the eye, rather than being proposed as a firm causal
31 connection.
32

33 **Figure 9.** CASE STUDY 2 (East to West) Temporal development of the particle size
34 spectra plotted along the 5 day back trajectory shown in plotted green/red
35 from midnight to midnight on the particle number (PN) emission map shown
36 in panel (b), starting at KPO on 11th of April 2008 and arriving at MHD on the
37 16th of April 2009 at 18:00. Spectra collected from the nearest site to the air
38 mass path is plotted in the left middle and left bottom panels (c, e). The peak
39 fitted the modal diameters and area of each of these curves is shown on the
40 middle and right hand panels (d, f). The middle panels correspond to the
41 metrics derived from the number spectra and the lower panels correspond to
42 the metrics derived from the volume spectra. The dotted lines in panels (c)
43 and (e) are primarily to guide the eye, rather than being proposed as a firm
44 causal connection.
45

46 **Figure 10.** CASE STUDY 3 (South to North) Temporal development of the particle size
47 spectra plotted along the 5 day back trajectory shown in plotted green/red
48 from midnight to midnight on the particle number (PN) emission map shown
49 in pane (b), starting at JFJ-HPB on 2nd February 2008 and arriving at ZEP on
50 the 7th of February 2008 at 06:00. Spectra collected from the nearest site to

1 the air mass path is plotted in the left middle and left bottom panels (c, e).
2 The peak fitted the modal diameters and area of each of these curves is
3 shown on the middle and right hand panels (d, f). The middle panels
4 correspond to the metrics derived from the number spectra and the lower
5 panels correspond to the metrics derived from the volume spectra. The
6 dotted lines in panels (c) and (e) are primarily to guide the eye, rather than
7 being proposed as a firm causal connection.
8

9 **Figure 11.** CASE STUDY 4 (North to South) Temporal development of the particle size
10 spectra plotted along the 5 day back trajectory shown in plotted green/red
11 from midnight to midnight on the particle number (PN) emission map shown
12 in panel (b), starting at PAL on 11th October 2009 and arriving at CMN on the
13 17th of October 2009 at 18:00. Spectra collected from the nearest site to the
14 air mass path is plotted in the left middle and left bottom panels (c, e). The
15 peak fitted the modal diameters and area of each of these curves is shown
16 on the middle and right hand panels (d, f). The middle panels correspond to
17 the metrics derived from the number spectra and the lower panels
18 correspond to the metrics derived from the volume spectra. The dotted lines
19 in panels (c) and (e) are primarily to guide the eye, rather than being
20 proposed as a firm causal connection.
21

1 **Table 1. Locations and names of stations used in the data analysis. The site altitudes are**
 2 **given with reference to standard sea level. The areas are grouped by European sub-**
 3 **divisions using definitions from Central Intelligence Agency (2009). Country codes are**
 4 **given in the ISO 3166 standard.**

| Station name | Station code | Country | Coordinates, altitude (lat., lon., height.) | Site Type | Instrument |
|-------------------------------------|--------------|---------|---|-----------------------------------|------------|
| <i>Nordic and Baltic</i> | | | | | |
| Aspvreten | ASP | SE | 58°48'N, 17° 23'E, 30 m | | DMPS |
| Birkenes | BIR | NO | 58°23'N, 8°15'E, 190 m | Mostly remote | DMPS |
| Pallas | PAL | FI | 67° 58'N, 24°7'E, 560 m | Remote | DMPS |
| Preila | PLA | LT | 55°55'N, 21°0'E, 5 m | Weakly influenced, general remote | SMPS |
| SMEAR II | SMR | FI | 61°51'N, 24°17'E, 181 m | Mostly remote | DMPS |
| Vavihil | VHL | SE | 56°1'N, 13°9'E, 172 m | Rural | DMPS |
| <i>Central Europe</i> | | | | | |
| Bösel | BOS | DE | 53°N, 7°57'E, 16 m | Rural | SMPS |
| K-Puszt | KPO | HU | 46°58'N, 19°19'E, 125 m | Rural | DMPS |
| Melpitz | MPZ | DE | 51°32'N, 12°12'E, 87 m | Rural | DMPS |
| Kosetice | OBK | CZ | 49°35'N, 15°15'E, 534 m | Rural | SMPS |
| Hohenpeissenberg | HPB | DE | 47°48'N, 11°11'E, 988 m | Rural | SMPS |
| Waldhof | WAL | DE | 52°31'N, 10°46'E, 70 m | Rural | SMPS |
| <i>Western Europe</i> | | | | | |
| Cabauw | CBW | NL | 51°18'N, 4°55'E, 60 m | Agglomeration | SMPS |
| Harwell | HWL | UK | 51°34'N, 1°19'W, 60 m | Agglomeration | SMPS |
| Mace Head | MHD | IE | 53°19'N, 9°53'W, 5 m | Generally remote | SMPS |
| <i>Mediterranean</i> | | | | | |
| Finokalia | FKL | GR | 35°20'N, 25°40'E, 250 m | Mostly remote | SMPS |
| JRC-Ispra | IPR | IT | 45°49'N, 8°38'E, 209 m | Agglomeration | DMPS |
| <i>Arctic</i> | | | | | |
| Zeppelin | ZEP | NO | 78°55'N, 11°54'E, 474 m | Remote | DMPS |
| High Altitude sites (over 1000 msl) | | | | | |
| <i>Western Europe</i> | | | | | |
| Puy de Dôme | PDD | FR | 45°46'N, 2°57'E, 1465 m | Weakly influenced | SMPS |
| <i>Central Europe</i> | | | | | |
| Schauinsland | SSL | DE | 47°55'N, 7°55'E, 1210 m | Rural | SMPS |
| Zugspitze | ZSF | DE | 47°25'N, 10°59'E, 2670 m | Weakly influenced | SMPS |
| Jungfrauoch | JFJ | CH | 46°32'N, 7°59'E, 3580 m | Mostly remote | SMPS |
| <i>Balkans</i> | | | | | |
| BEO Moussala | BEO | BG | 42°10'N, 23°35'E, 2971 m | Mostly remote | SMPS |
| <i>Mediterranean</i> | | | | | |
| Monte Cimone | CMN | IT | 44°11'N, 10°41'E, 2165 m | Weakly influenced | DMPS |

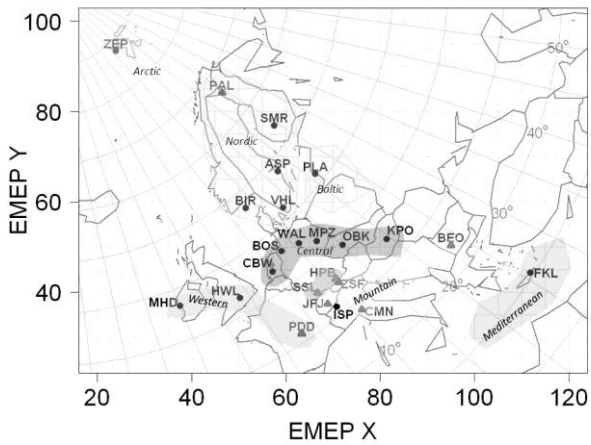
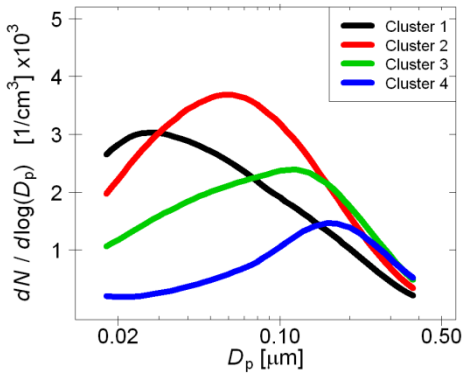
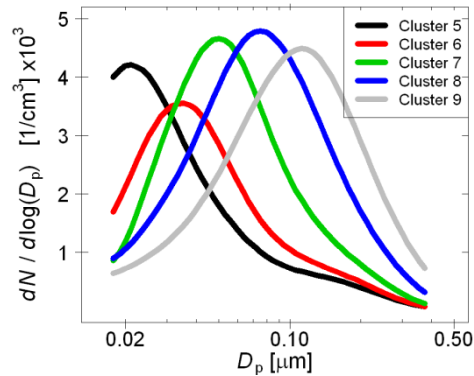


Figure 1. Location of the 24 EUSAAR and GUAN stations in Table 1

1
2
3



(a)



(b)

Figure 2. Average Cluster Spectra resulting from the cluster analysis of the daily mean spectra collected at each of the 24 EUSAAR sites. (a) Clusters 1, 2 and 3 are the broad central European spectra and the Arctic spectrum 4 and (b) Clusters 5, 6, 7, 8 and 9 are the narrower size distributions observed at sites outside of the central European area.

4
5
6
7
8
9
10
11
12

Outpost sites.

Nordic + Westerly sites

Central Europe sites

Mountain sites

Low Latitude + Mountain sites

High longitude sites

North to South

West to East

West to East

North to South

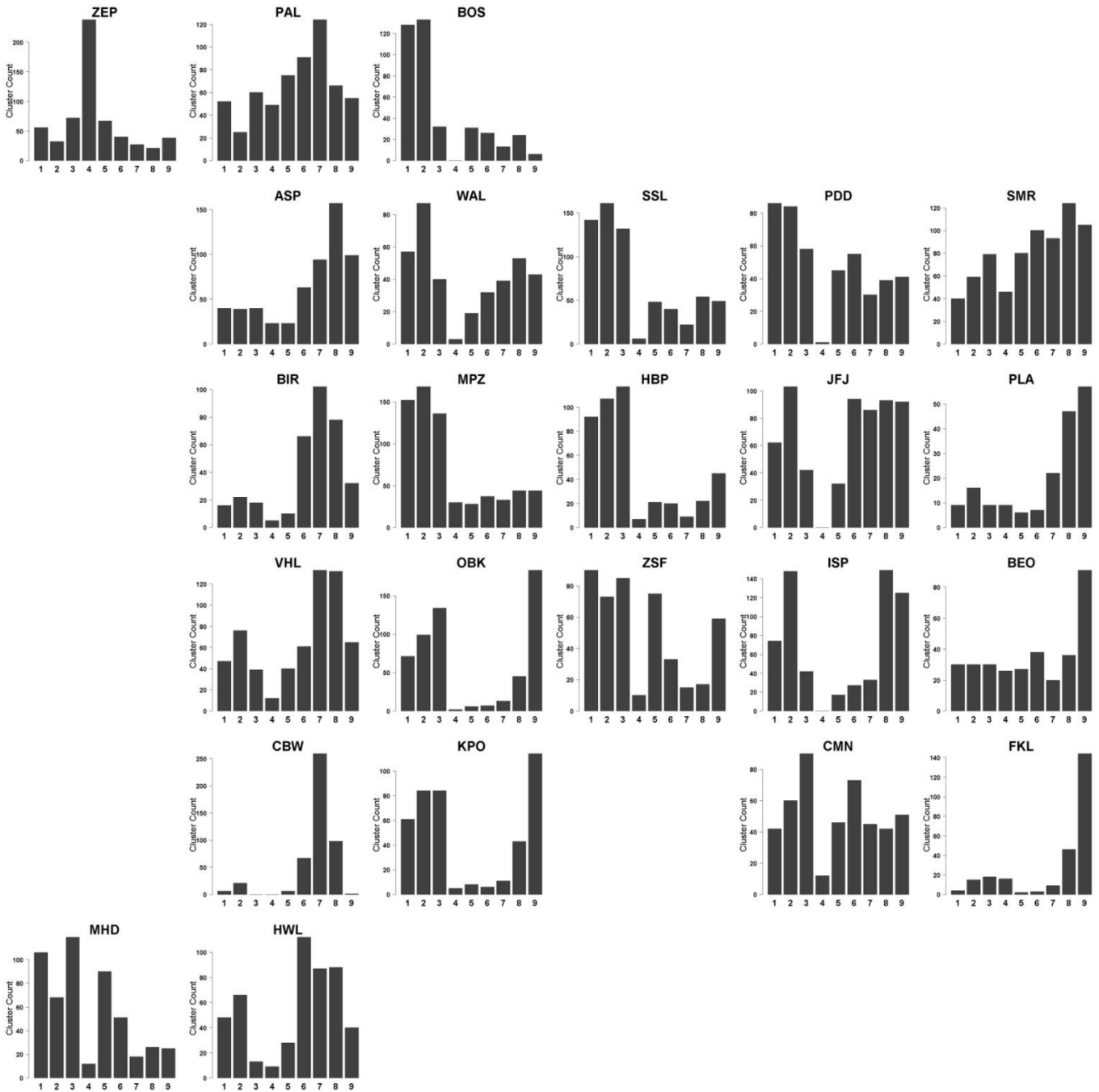
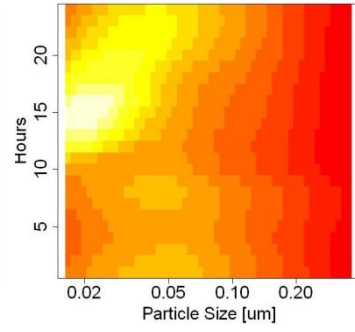
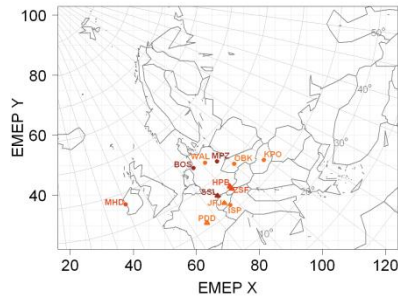
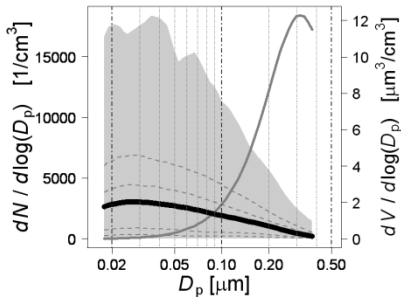


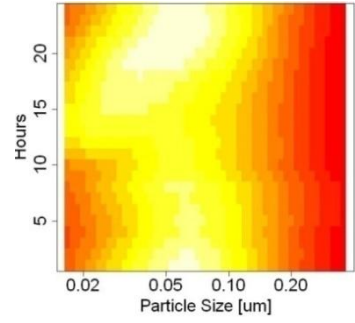
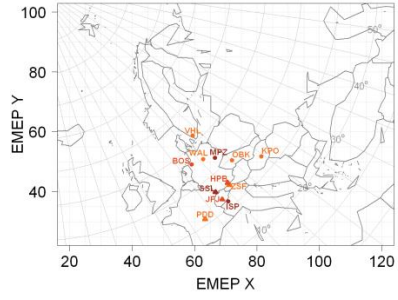
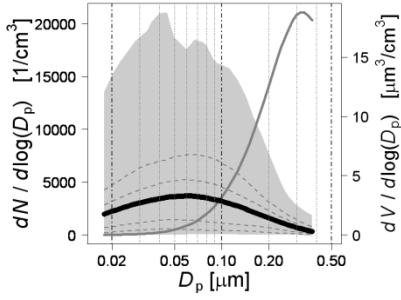
Figure 3. Frequency of the clusters measured at each of the sites arranged in columns of similar patterns.

1

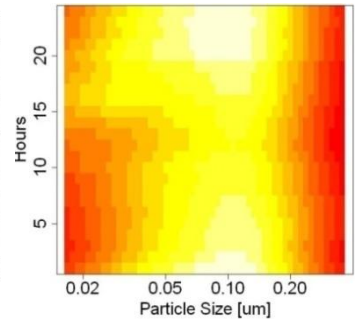
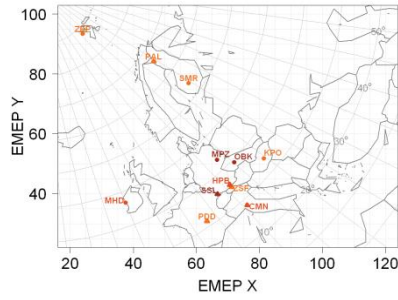
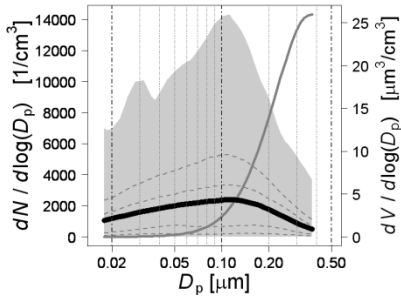
2



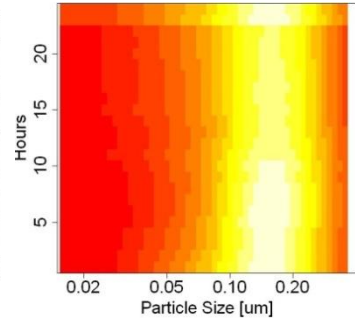
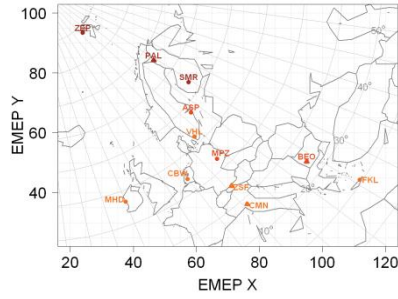
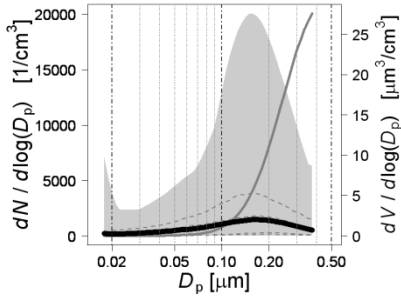
1



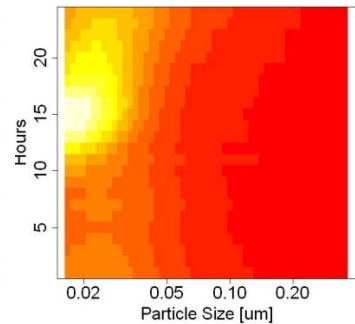
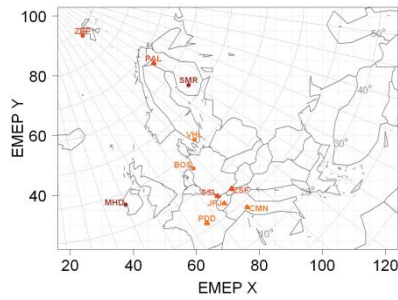
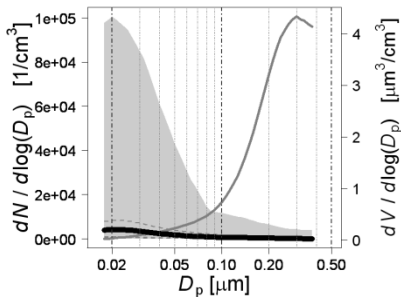
2



3



4



5

1
2
3
4

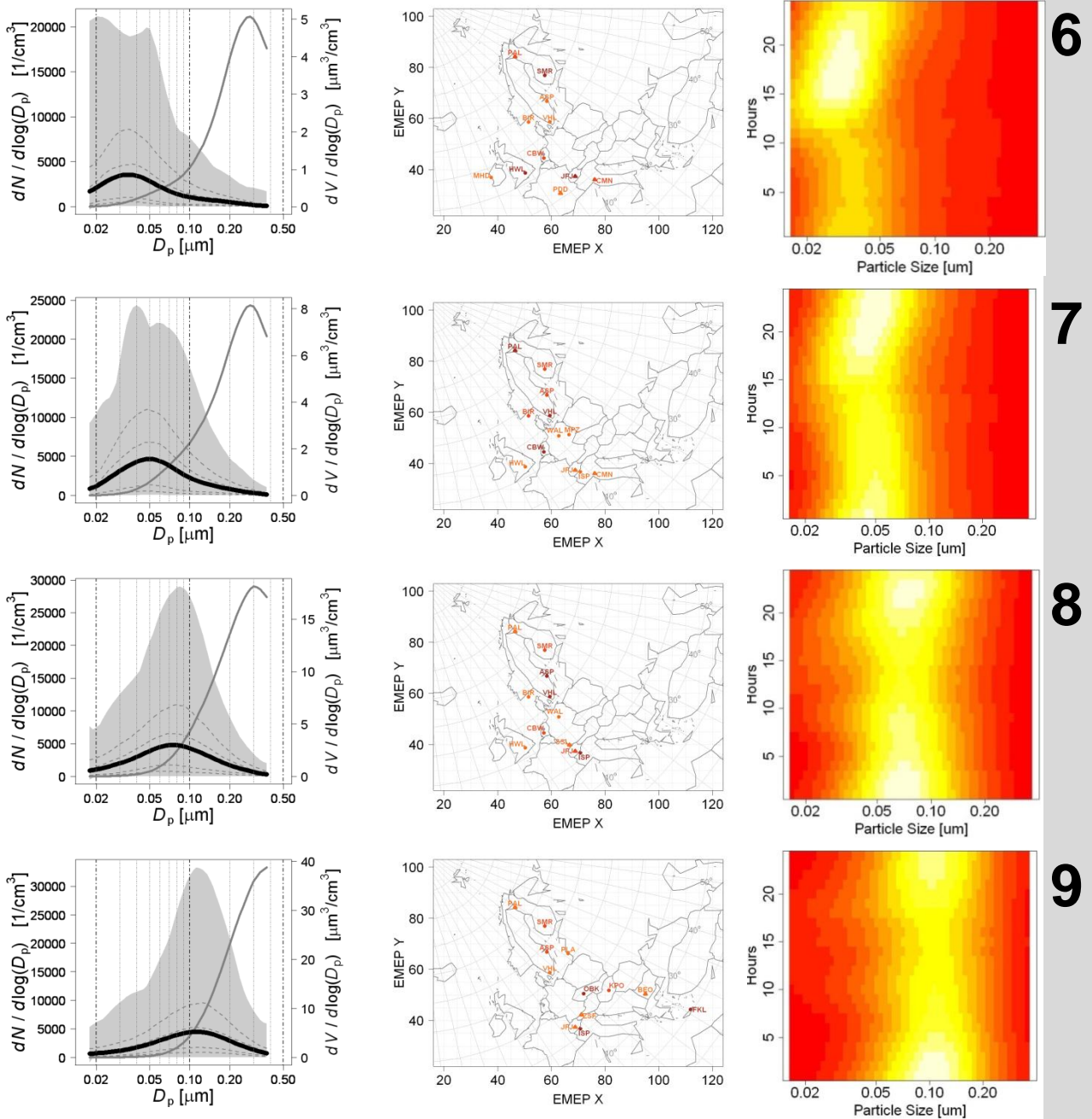


Figure 4. Average clustered particle size distributions (*cluster 1-9 left hand panels*) and the spatial distribution of each cluster (*centre panels*). The solid black line shows the average spectrum and the dashed lines show the 10th, 25th, 75th and 90th percentile spectrum. The maximum and minimum spectra are traced out by the extremities of the shaded areas. The middle panels show where each of the clusters are most likely to be detected. When counting the spectrum types within the whole data set, the sites which collected above the 90th, 75th and 50th percentile were marked with a progressively lighter orange colour (see Figure S5 for the frequency distributions). Circles denote boundary layer sites and triangles denote sites of relatively high altitude. The right hand panel shows the colour maps plotted using the average day of hourly spectra for each of the clusters. [The shade from red-yellow-whites represent a linear scale of $dN / d\log(D_p)$ between the minimum value of the 10th percentile spectrum and the maximum value of the 90th percentile spectrum shown for each cluster.]

1

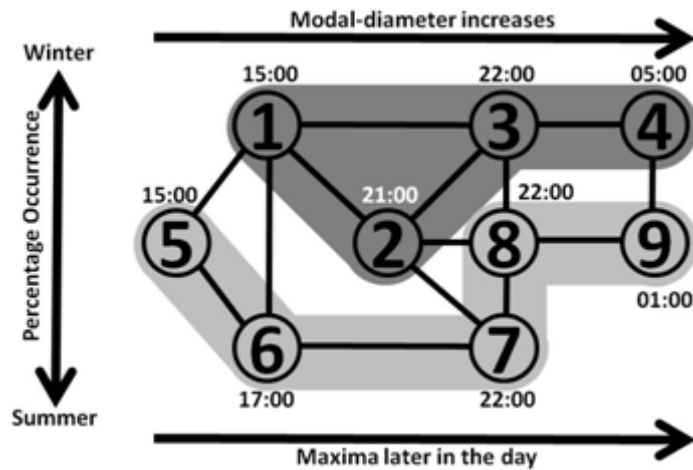


Figure 5. Cluster Proximity Diagram. Each node in the diagram represents a cluster and each cluster is arranged according to its similarity to its neighbour. The modal diameter increases from left to right across the diagram and the two shaded regions indicate those clusters which are most frequently detected in central Europe (dark grey) and those which are not (lighter shades of grey). The times positioned next to each node indicate when the maximum particle number concentration of each cluster occurred.

2

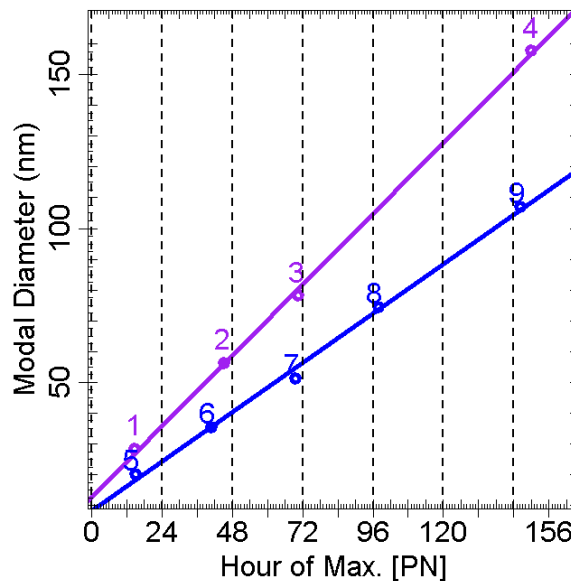


Figure 6. Plot showing how the modal diameters MD of the average cluster spectra vary with the hour HR of their maximum particle number concentration [PN]. The purple (1,2,3 and 4) and blue (5,6,7,8 and 9) colours depict two aggregated trends observed in the data based on a South to North and West to East air mass movement. The rates of growth from cluster to cluster are: for the purple (1, 2, 3 and 4) 0.9, 0.9 and 1.0 nm / hr; and for the blue (5, 6, 7, 8 and 9) equal 0.59, 0.55, 0.82 and 0.67 nm / hr [Fitted lines: $y = 0.96x + 12.8$ and $y = 0.67x + 8.11$]

3

4

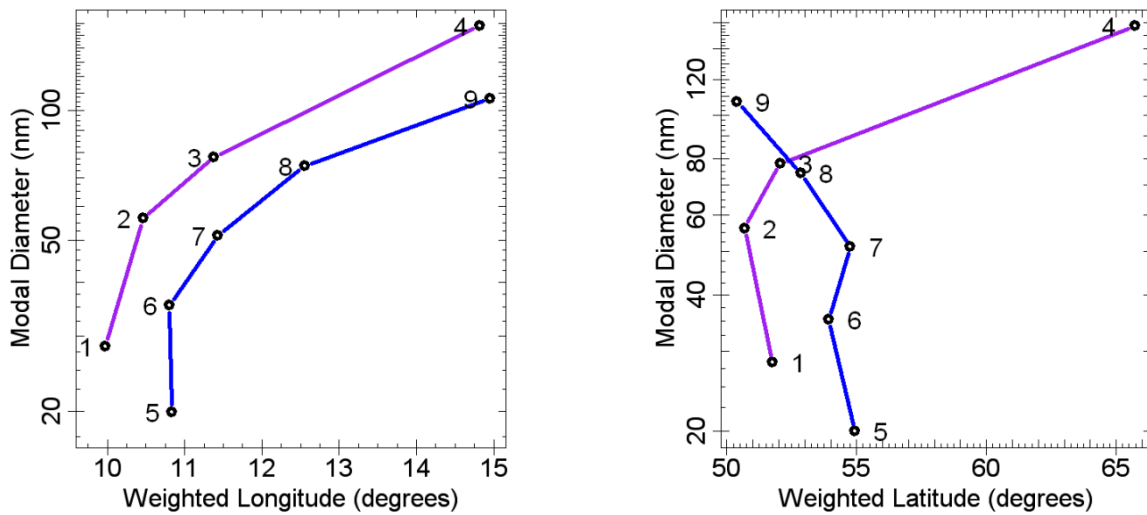
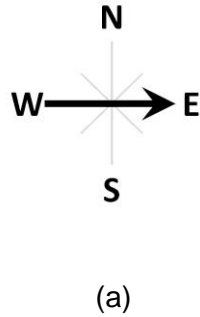
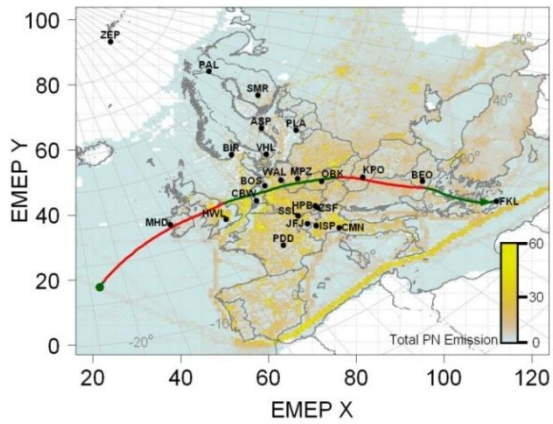


Figure 7. Using the number distribution, the fitted modal diameter of each cluster (1-9) is plotted against the Weighted Longitude or Latitude, calculated for each cluster, using $WL = \frac{\sum_i^{24} W_i \cdot X_i}{\sum_i^{24} W_i}$, where X_i is the latitude/longitude of the sites where the cluster is detected and W_i is the corresponding population of the cluster across the 24 sites. The purple (1,2,3 and 4) and blue (5,6,7,8 and 9) colours depict two aggregated trends observed in the data based on a South to North and West to East air mass movement.

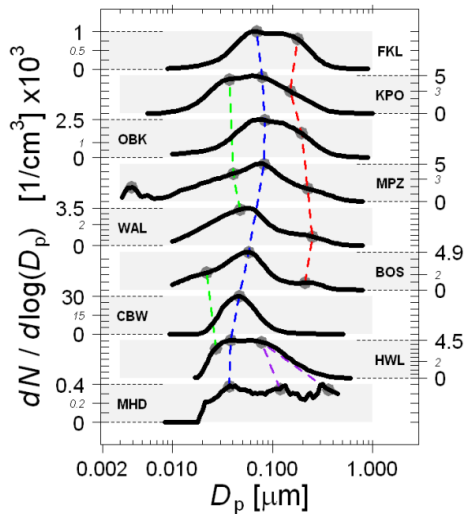
- 1
- 2
- 3
- 4
- 5
- 6
- 7
- 8
- 9
- 10
- 11
- 12
- 13
- 14
- 15
- 16
- 17
- 18
- 19



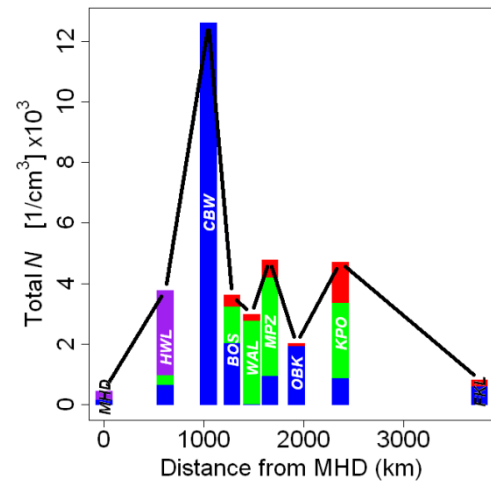
(a)



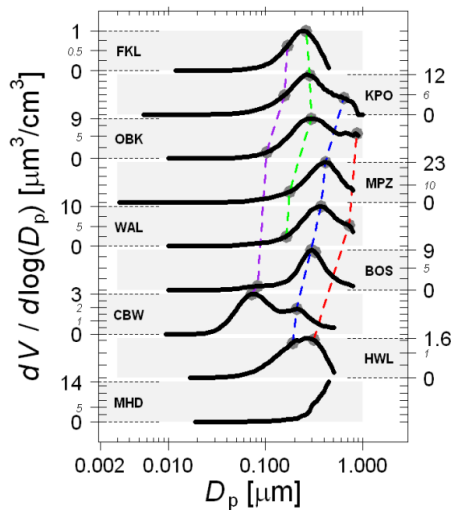
(b)



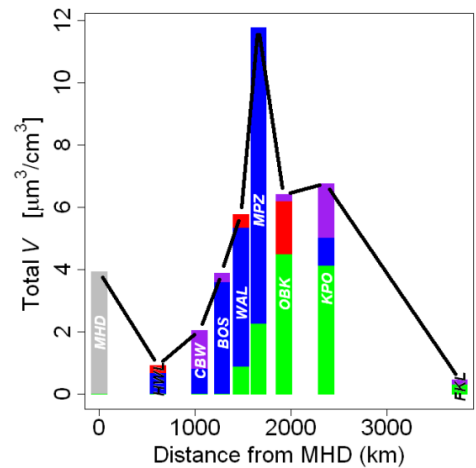
(c)



(d)

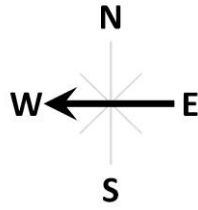


(e)

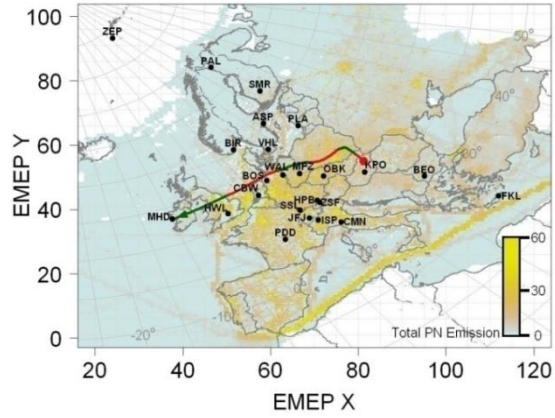


(f)

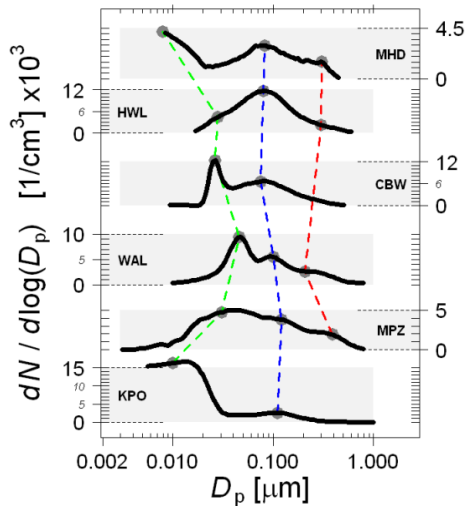
1 **Figure 8. CASE STUDY 1 (West to East) Temporal development of the particle size spectra**
 2 **plotted along the 5 day back trajectory shown in plotted green/red from midnight to**
 3 **midnight on the particle number (PN) emission map shown in panel (b), starting southwest**
 4 **of MHD on 18th December 2008 and arriving at FKL on 24th December 2008 at 0:00. The**
 5 **stacked number and volume spectra (c, e) show the size distributions measured at the sites**
 6 **as the air mass passes. The modal diameter of the fitted distributions are indicated by**
 7 **circles and the progress plotted by the coloured lines which are coded to indicate the**
 8 **fraction of total number for each site plotted against distance in the right hand panels (d, f).**
 9 **The dotted lines in panels (c) and (e) are primarily to guide the eye, rather than being**
 10 **proposed as a firm causal connection.**



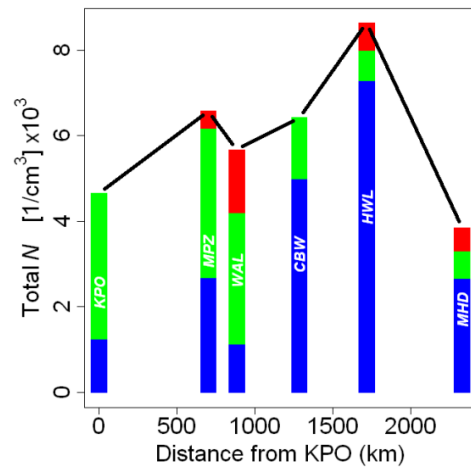
(a)



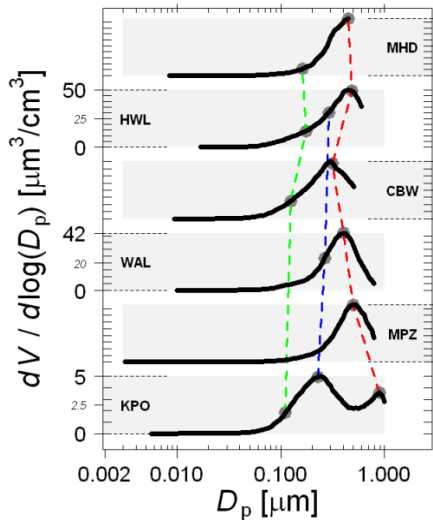
(b)



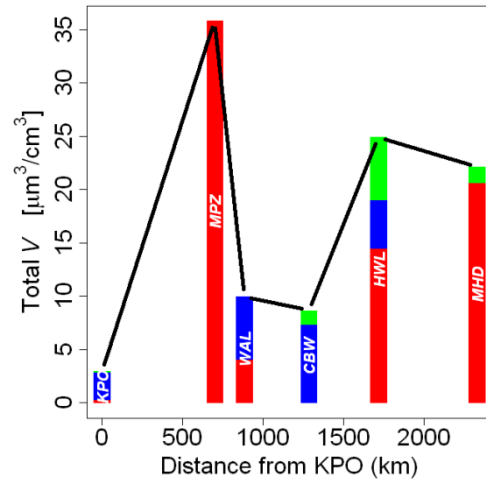
(c)



(d)

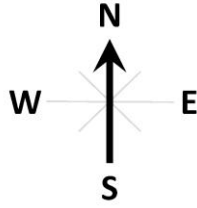


(e)

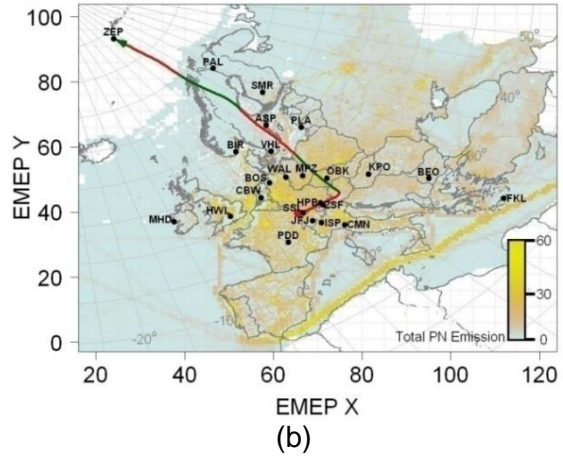


(f)

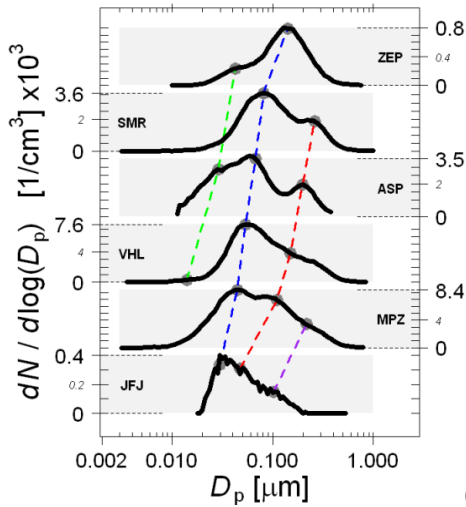
1 **Figure 9. CASE STUDY 2 (East to West) Temporal development of the particle size spectra**
 2 **plotted along the 5 day back trajectory shown in plotted green/red from midnight to**
 3 **midnight on the particle number (PN) emission map shown in panel (b), starting at KPO on**
 4 **11th of April 2008 and arriving at MHD on the 16th of April 2009 at 18:00. Spectra collected**
 5 **from the nearest site to the air mass path is plotted in the left middle and left bottom panels**
 6 **(c, e). The peak fitted the modal diameters and area of each of these curves is shown on**
 7 **the middle and right hand panels (d, f). The middle panels correspond to the metrics**
 8 **derived from the number spectra and the lower panels correspond to the metrics derived**
 9 **from the volume spectra. The dotted lines in panels (c) and (e) are primarily to guide the**
 10 **eye, rather than being proposed as a firm causal connection.**



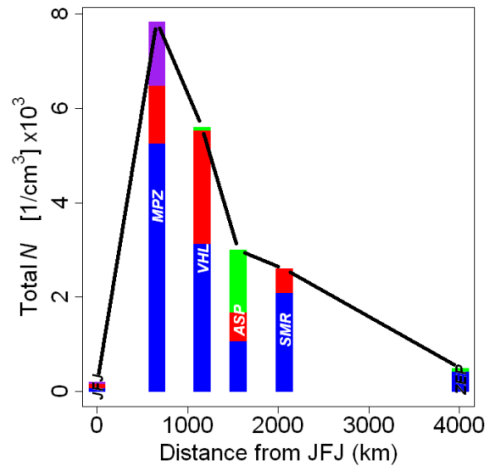
(a)



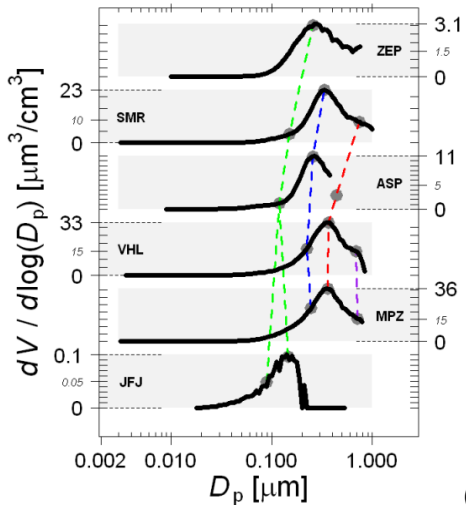
(b)



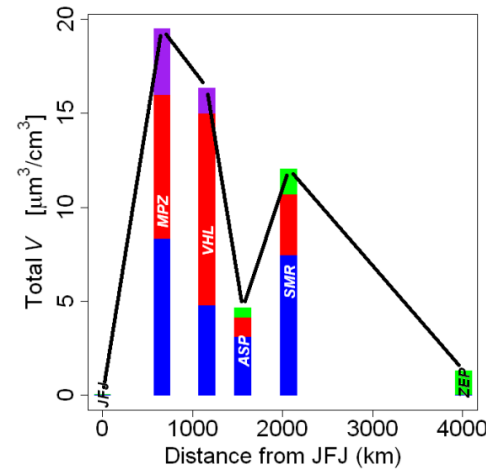
(c)



(d)

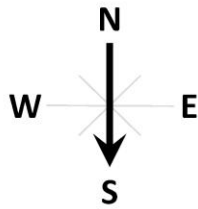


(e)

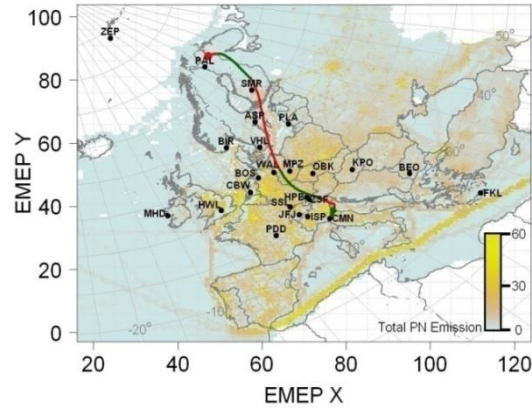


(f)

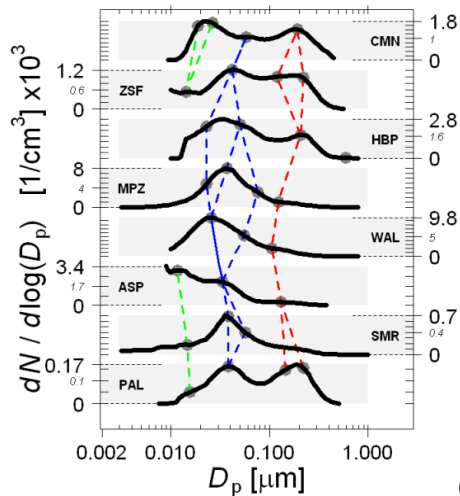
1 **Figure 10. CASE STUDY 3 (South to North) Temporal development of the particle size**
 2 **spectra plotted along the 5 day back trajectory shown in plotted green/red from midnight to**
 3 **midnight on the particle number (PN) emission map shown in pane (b), starting at JFJ-HPB**
 4 **on 2nd February 2008 and arriving at ZEP on the 7th of February 2008 at 06:00. Spectra**
 5 **collected from the nearest site to the air mass path is plotted in the left middle and left**
 6 **bottom panels (c, e). The peak fitted the modal diameters and area of each of these curves**
 7 **is shown on the middle and right hand panels (d, f). The middle panels correspond to the**
 8 **metrics derived from the number spectra and the lower panels correspond to the metrics**
 9 **derived from the volume spectra. The dotted lines in panels (c) and (e) are primarily to**
 10 **guide the eye, rather than being proposed as a firm causal connection.**



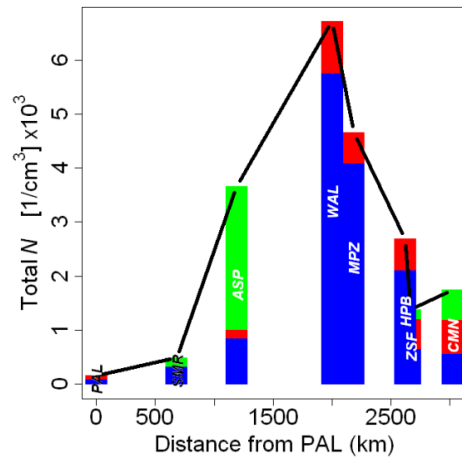
(a)



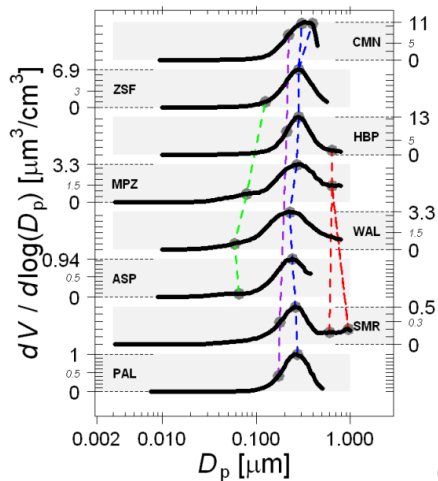
(b)



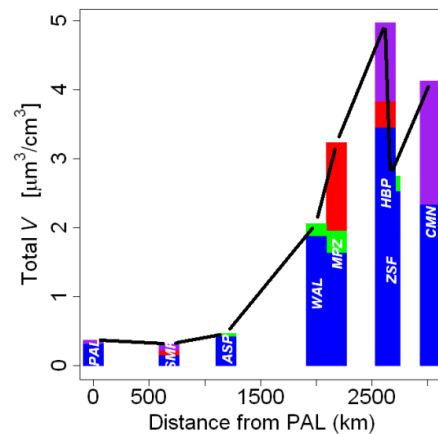
(c)



(d)



(e)



(f)

2

3 **Figure 11. CASE STUDY 4 (North to South) Temporal development of the particle size**
 4 **spectra plotted along the 5 day back trajectory shown in plotted green/red from midnight to**
 5 **midnight on the particle number (PN) emission map shown in panel (b) starting at PAL on**
 6 **11th October 2009 and arriving at CMN on the 17th of October 2009 at 18:00. Spectra**
 7 **collected from the nearest site to the air mass path is plotted in the left middle and left**
 8 **bottom panels (c, e). The peak fitted the modal diameters and area of each of these curves**
 9 **is shown on the middle and right hand panels (d, f). The middle panels correspond to the**
 10 **metrics derived from the number spectra and the lower panels correspond to the metrics**
 11 **derived from the volume spectra. The dotted lines in panels (c) and (e) are primarily to**
 12 **guide the eye, rather than being proposed as a firm causal connection.**